Recent advances in studying single bacteria and biofilm mechanics

Catherine Even, Christian Marlière, Jean-Marc Ghigo, Jean-Marc Allain, Alba Marcellan, Eric Raspaud

Recent advances in studying single bacteria and biofilm mechanics.

Catherine Even[a], Christian Marlière[b], Jean-Marc Ghigo[c], Jean-Marc Allain[d,e], Alba Marcellan[f], Eric Raspaud[a]

[a] Laboratoire de Physique des Solides, Université Paris-Sud, CNRS, Université Paris-Saclay, 91405 Orsay Cedex, France.

[b] Institut de Chimie Moléculaire et des Matériaux d'Orsay, CNRS, Université Paris-Sud, Université Paris-Saclay, 91405 Orsay, France.

[c] Institut Pasteur, Unité de Génétique des Biofilms, 28 rue du Dr. Roux 75724, Paris cedex, France.

[d] LMS, École polytechnique, CNRS, Université Paris-Saclay, 91128 Palaiseau, France.

[e] Inria, Université Paris-Saclay, 91128 Palaiseau, France

[f] Laboratoire Sciences et Ingénierie de la Matière Molle, PSL Research University, UPMC Univ Paris 06, ESPCI Paris, CNRS, 10 rue Vauquelin, 75231 Paris cedex 05, France.

Abstract

Bacterial biofilms correspond to surface-associated bacterial communities embedded in hydrogel-like matrix, in which high cell density, reduced diffusion and physico-chemical heterogeneity play a protective role and induce novel behaviors. In this review, we present recent advances on the understanding of how bacterial mechanical properties, from single cell to high-cell density community, determine biofilm tri-dimensional growth and eventual dispersion and we attempt to draw a parallel between these properties and the mechanical properties of other well-studied hydrogels and living systems.

Keywords (up to six): mechanics, bacteria, biofilm, growth, hydrogel, elasticity

Contents

1. Introduction

Bacteria-inspired physics cover many fields ranging from superfluidity [1] to topological defects [2]. The study of bacteria and surface attached, matrix-enclosed multicellular communities called biofilms using biophysics concepts and tools recently received much

attention from the physics and physical chemistry communities. As noted by Wilking *et al.* in 2011, soft matter physics can be used to described biofilm: rigid colloidal-like bacteria are embedded in an extracellular matrix resembling a chemical polymer gel, forming a solid composite biomaterial [3].

One of the most characteristic biological features that distinguish biofilms from planktonic populations is the presence of a self-produced extra-cellular matrix composed of a mix of polysaccharides, water, ions, DNA, proteins released by biofilm bacteria and forming some supramolecular structures [4,5]. These compounds are considered as the building blocks structuring biofilm communities, which can reach size ranging from micrometers to several centimeters (Figure 1, [6,7]), and are able to colonize very large surface areas in almost all known natural or artificial environments.

Indeed, multi-species biofilms are found in most natural or industrial settings and represent a predominant bacterial lifestyle from which individual bacteria constantly disseminate. Bacteria display a remarkable plasticity and are able to sense and respond to many external stimuli in order to adapt to their environments. Whereas microbiology mostly focused so far on the influence of the chemical environment on bacterial behavior, passive and active bacterial responses to physical stimuli and mechanical cues have been only recently recognized to also change bacterial behaviors [8].

Since 2011 [3], the number of reviews on biofilm mechanics demonstrates the growing interest of the community [8,9,10,11,12]. However, “the mechanical world of bacteria” [8] has only been partially explored and the aim of the present review is to highlight recent results on bacterial mechanics. We report the different experimental approaches of bacterial mechanics at a single cell level and at the level of multicellular, heterologous biofilm,

replacing biofilm studies within the more general context of living tissues and synthetic hydrogels.

2. Mechanics of single bacteria

Most mechanical studies on single bacteria focus on bacteria hydrodynamics (see for instance [13]), on their rigidity or on the mechanical forces exerted by its organelles. However, mechanical forces also play a major role in bacterial locomotion, chromosome segregation, or cell wall remodeling among other phenomena [14]. In this review, we have chosen to focus on mechanical properties of cell-envelope and cell-wall, on mechanosensors, and, after briefly introducing bacterial flagella and the different bacterial modes of locomotion, on pili mechanics and on cell adhesion/detachment processes. Table 1 reports the main typical values described in this section 2.

2.1. Bacterial cell envelope

Stiffness is traditionally quantified by the Young's modulus (YM) value. Experimental [15] and theoretical studies [16] have reported a large dispersion of YM values for bacterial cells. It simply reflects the heterogeneous composition of the cell envelope constituted in most bacteria by one or two layers of membrane, a rigid cell wall consisting of a network of peptidoglycan (PG) polymers and various appendices (pili,etc…). These components have different deformation values when loads are applied leading to a large dispersion in elastic modulus values [16]. The large concentration of solutes in the cytoplasm generates an osmotic pressure, termed turgor pressure, which is constrained by the cell wall thus defining the cell shape.

Currently, AFM is the direct technique well-suited for probing forces on microbial cells, both at the single cell and single-molecule levels [17]. A standard or functionalized AFM tip can be used to probe mechanical properties of bacteria at nanometric scale [18]. Due to the difficulties for separating the contributions of the wall and turgor pressure to the mechanical response, most mechanical measurements on the cell wall have been performed using chemically isolated walls, termed saccule. Figure 2A shows a typical AFM measurement performed on isolated *Pseudomonas aeruginosa* in liquid environment and illustrates modification of cells stiffness in presence of antibiotics, their Young's Modulus (YM) dropping strongly after treatment by two antibiotics from 270 kPa to 50 and 25 kPa [15,19,20]. For wild type strains (NCTC 8325-4) of *Staphylococcus aureus*, YM values may range from 50 kPa [16] to few MPa values [21]. In the case of *Staphylococcus epidermidi*s strains with various abilities to produce extracellular material, YM may vary from 8 kPa to 22 kPa. Different mechanical responses were also detected for non-fibrillated (13 kPa) or fibrillated (7 kPa) strains of *Streptococcus salivarius* [16]. Whole-cells elasticity has also been measured on many different bacteria, including *Myxococcus xanthus* [22] and *E. coli* [23] among others, and was found to be within the same orders of magnitude, ranging between few kPa to several MPa.

It should be noted that precise mapping of the cell stiffness at high resolution by AFM can also reveal the presence of other types of bacterial components. As shown in Figure 2B and C, the extracellular secreted substances of low stiffness are clearly distinguishable from high bacterial stiffness [18]. Another example is the capsule, a polysaccharide layer that lies outside the bacterial cell wall of given strains and which may be very resistant to external agent as antiseptic and surfactant. AFM measurements of capsule thickness revealed that the wild-type *Klebsiella pneumoniae* capsule was rearranged by exposure to colistin, a polypeptide antibiotics [24].

Other technics were also used to determine the mechanical properties of whole cells. Optical tweezer bending experiments were performed on *Borrelia burgdorferi* cells giving stiffness values of same order of magnitude [25]. Microfluidic devices were also specifically designed. By modulating the fluid flow, it was possible to apply variable hydrodynamic forces on the live cells in order to deform them under different environmental conditions to control their growth conditions. The technics allowed to measure the flexural rigidity of cells in various physiological states [26]. In a specific microfluidic platform with sub-micron features, individual bacteria were flowed and trapped in tapered channels [27]. Less stiff bacteria undergo greater deformations and therefore travel further into the tapered channel. Hence, the distance traversed by bacteria into the tapered channel is inversely related to cell stiffness that can consequently be determined.

2.2. Cell wall

The cell wall is mainly a network of long sugar strands (glycans) crosslinked by stretchable peptides, the so-called peptidoglycan (PG). This network envelops bacteria forming a quite thin shelter sandwiched by two fluid membranes in Gram-negative while being thicker and in direct contact with the external environment in Gram-positive bacteria. The rigid cell wall protects bacteria and gives them their shape and mechanical integrity as it serves as the primary structure for bearing the osmotic stress named the turgor pressure [28,29,30]. The turgor pressure results from all the internal cytoplasmic components that press against the cytoplasmic membrane or against the cell wall. It typically ranges for *E. coli* between 0.5 to 3 atm (atmosphere) depending on the osmolality of surrounding growth medium [31]. Changes in structure and elasticity of PG were studied by AFM on *Streptococcus* cells subjected to increasing turgor pressure by variation of the medium osmolality [32]. The authors show a

new net-like arrangement of PG which stretches and stiffens following osmotic changes. The primary source of substantial mechanical stress in the bacterial cell wall is therefore the turgor pressure.

Importantly, the cell wall is a structure in constant evolution, as peptidoglycan bonds must be broken to permit growth or division, with a risk of the appearance of defects in the peptidoglycan network. This could lead to the lysis of cells unable to withstand osmotic pressure. As many antibiotics target the growing cell wall, several studies tried to get a quantitative understanding of the cell sensitivity to defects in the cell wall. For example vancomycin antibiotic often leads to the formation of noticeable bulges which grew with time and led eventually to cell lysis. In order to detect the ‘‘chemical features’’ of bacterial cell wall and their modifications with external agents, a surface-enhanced Raman scattering (SERS) technique was developed and applied to assess the fine structures of the bacterial cell wall [33]. The declines in some SERS peaks seem to be indicative of a slowing in Gram negative bacterial growth in the early phase of the ampicillin treatment. This high-speed SERS detection represents an original approach for microbial diagnostic, which could be applied to a single bacterium.

Much attention was paid on the genes and proteins involved in synthesis of the bacterial cell wall [34]. The MreB protein forms extended filamentous structures and interacts with multiple components of the cell wall synthetic machinery. It is one of the main geometric regulators (determination and maintenance) of the rod-cell shape in Gram-negative bacteria. Different models have been recently proposed to describe the wall growth and the local remodeling while maintaining the rod shape of cells (Figure 3) [35,36]. Using standard fluorescence microscopy, early images of MreB localization revealed long helical filaments that follow a helical path along the periphery of the cell. They have suggested a direct role of MreB in governing cell wall architecture. These filaments were reported to be dynamic as

they were seen to rotate around the long axis of the cell in some experiments. Their dynamics was then assumed to be actin-like and to follow a helical pattern of insertion of new peptidoglycans [37,38,39]. However, several more recent studies, using cutting-edge optical microscopy technics with much higher spatial and temporal resolutions [40,41,42], have questioned this point of view, as the movement of the involved proteins appears more circumferential than helical and depends on on-going peptidoglycan synthesis rather than on actin-like polymer dynamics [34].

Mechanical models have also been proposed to explain cell bulging or cell separation. Models of the bulging mechanics of the cytoplasmic membrane through pores in the cell wall have predicted a critical pore radius beyond which spontaneous bulging will occur in reasonable agreement with the observed distribution of pores in the peptidoglycan network [30]. Another prediction of these models is that the critical pore radius would increase with increasing surface tension and decrease with increasing spontaneous curvature or turgor pressure, suggesting that bulging may depend on the lipid composition of the membrane and the metabolic state of the cell [30]. Boulbitch *et al.* [43] have modeled the cell wall as a deformable hexagonal mesh and they predicted a load-dependent elasticity with a power-law stress-stiffening exponent around 1. Thwaites *et al.* used standard fiber-measuring technique on *Bacillus subtilis*, a Gram-positive bacterium, with a thick cell wall consisting of 50% peptidoglycan by weight. They found a change of one order of magnitude in the thread modulus upon loading [44,45]. A bacterial thread is the common name given to a multifilament fiber produced from cultures of a cell-separation suppressed mutant of *Bacillus subtilis* [44].

By studying intact and bulging *E. coli* cells with AFM, the contributions of the cell wall and of the turgor pressure to the overall cell stiffness were obtained independently [46]. Figure 3B illustrates the stiffness drop when indenting an *E. coli* cell and the bulge. A 30 kPa turgor

pressure was found in intact living cells while lower turgor pressures were calculated in bulging cells from the bulge characteristics. The lower the pressure the lower the radius and stiffness of bacteria in bulging cells. The wall was shown to be significantly stiffer in intact cells: few tens of MPa depending on the observation (axial or circumferential) directions than in unpressurized sacculi. The authors found strong evidence of stress stiffening in the cell wall and incorporated nonlinear elasticity of the peptidoglycan network as a power-law in the turgor pressure [46].

Finally modeling the mechanics of separating daughter cells with finite element analysis has been recently reported [47]. The authors have suggested that a mechanical crack propagation of the cell wall drives millisecond cell separation in round *Staphylococcus aureus*. As illustrated in Figure 3C and D, high stress localizes at the peripheral ring and prepares cell for popping. Increasing the turgor pressure and the cell wall stress by lowering the medium osmolarity results in an enrichment of the popping events.

2.3. Mechanosensors

Mechanosensitive (MS) channels are fundamental components of bacterial cells [48,49] as they maintain a positive turgor pressure, estimated to range between 2 and 4 atm [50,51] in *E. coli* and enable the preservation of physical integrity during osmotic shock due to hypothetic variations of ionic strength of liquid environment [52]. Cell integrity is maintained through the interplay between the peptidoglycan cell-wall, which provides a constraining force, and mechanosensitive (MS) channels that modulate turgor pressure by varying ion fluxes [52]. The mechanical membrane tension should not exceed around 15 mN/m to prevent the membrane rupture and the subsequent bacterial lysis [53,54,55].

MS channels are ubiquitous in bacterial world. They divide in two main families, MscS and MscL. MscL is a highly conserved, almost ubiquitous, membrane protein. MscS exists in

numerous variant forms that are united by the presence of a ‘pore-forming’ domain close to the carboxy-terminal end of the protein [56]. Bacterial strains differ in the number of MS channels they possess, some having only few, whereas others, for example the γ-proteobacteria have up to six MscS homologues in addition to MscL [57].

To retain structural integrity of the cell during pressure transitions, MS channels gate on the millisecond time-scale to release large-amount of solutes whenever the net outward pressure generates an increase in membrane tension [58]. The experimental study of the activation of the MS channels is a difficult task when working with complete cells because of the presence of the peptidoglycan cell wall and the linked outer membrane but, in isolated membrane patches, pressures as low as approximately 0.05 atm were proved to activate MS channels [57,55].

2.4. Pili

Many bacterial cells display nano and/or micrometer long surface proteinaceous appendages (pili, fimbriae, flagella). These surface structures are important for cellular functions such as motility, adhesion to various inert or living surfaces and also intercellular communication. In particular, surface appendages of many bacteria are key factors during the first stages of colonization by promoting attachment to host cells as well as solid surfaces [59]. Depending on the growth environment, bacterial motility can be achieved by swimming in aqueous media, swarming, twitching and gliding on soft or hard solid surfaces [60]. Bacterial swimming motility usually involve flagellar motility while surface locomotion such as twitching motility involve specialized pili such as type IV pili, extension-retraction appendages that attach to points ahead and pull cells forward [61]. Swarming bacteria collectively move in groups using their flagella through a thin liquid layer on solid surfaces.

Gliding and sliding motilities do not need appendage but specialized membrane anchored macromolecular machines [62].

E. coli are known to express a large number of coilable pili [63,64,65,66,67] which help the bacteria to resist shearing forces in various host organs by reducing the instantaneous force on the adhesion. A well-studied example of pili is uropathogenic *E. coli* type 1 pili, which are essential for initiation of urinary tract and gastrointestinal infections. Since the width of type 1 pili is in the nanometer range, their study is therefore possible through the use of high resolution microscopy techniques such as electron microscopy, AFM or fluorescence analysis [68,69]. Thanks to these methods interesting information were brought in: numbers of pili on a cell, length of pili, pili rigidity, and so forth [70,71]. It was found that, similar to type 1 pili, P pili are highly extensible with an average 3 µm contour length and a 35 pN plateau force. The stiffness of the P pili is at least a few times larger than 0.15 pN/nm [72,73]. The results also suggest that physiological levels of shear flow (up to 90 pN/bacterium [74]) are likely to trigger unwinding of the helical region of both types of pili [75]. When exposed to an external force P and type 1 pili in *E. coli* can unwind their quaternary structure [76]. Another study reported a strong pH dependence of the maximal elongation of type 1 fimbriae when pulling living cells at different rates [77].

High-resolution force measurements, using optical tweezers and AFM were performed too. They have revealed macroscopic properties (such as force-extension behavior) and microscopic responses (e.g. transition energies and bond lengths) for several types of pili [73,78,79,80]. These studies provided a better understanding of the pili mechanics and supported the previous assumptions that pili are biopolymers capable of reducing the external load on the adhesins, at the origin of the initial attachment of bacteria and their adhesion on surfaces [76]. Flexible microscopic pillars can be used to measure the forces generated by pili as they can be deflected by pilus retraction [81]. If the pillar stiffness is known, then their

deflection can be measured by microscopy and converted into a force. This method is less sensitive at low forces and displacements but allows measurement of forces in the nanonewton range [82].

E. coli are rod-shaped bacterial cells with a typical length of 1−3 μm that express hundreds of pili, few micrometers long and 5−10 nm in diameter. A high amount of pili protruding out from the cell surface increases the surface area to mass per bacterium. In a fluid environment, this additional surface area causes an increased drag on the bacterium compared to a "bald" bacterium of the same size that does not express any pili. By remarking that surface organelles, even if they are very small, affect the fluid velocity around an object, optical tweezers (OT) experiments were recently proposed to study the change of the drag force on the cell with the fluid velocity and discriminate in real time and within seconds between single bacteria with and without pili [76].

Bacterial type IV Pili (T4P) are among the most powerful molecular motors characterized to date [83]. The dynamics of retraction and force generation properties of single or bundle of pili have been extensively studied. Laser tweezers (laser traps, optical tweezers) have proved useful for measuring the velocity of single pilus retraction and the force generated [83,84,85,86]. Measurements of displacements down to the subnanometer range and forces in the range of piconewtons can be achieved. It was shown that individual type IV pilus typically generates forces in the range of few tens of pN. These forces are higher than those generated by other molecular motors. However, the velocity of retraction (1–2 μms^{-1}) is in the same range as velocities of cytoskeletal motors.

AFM is particularly useful for characterizing the elastic properties of pili [87] where a bacterium is bound to a cantilever and is facing a surface. When a pilus binds to the opposite

surface this one can be displaced causing the application of a force on the pili. In this way, the extension of the pilus as a function of the applied force can be determined [87].

2.5. Adhesion/Detachment

Cell adhesion is mediated by various molecular interactions that are specific (i.e. through molecular recognition) or non-specific (i.e. hydrogen bonding, hydrophobic, van der Waals, electrostatic, etc.). Various biophysical assays have been developed for measuring biomolecular forces, including flow-chamber experiments, surface force apparatus, biomembrane force probe, magnetic and optical tweezers, and AFM [87, 88].

Another investigation method consists in gluing a unique living cell to the tip of the AFM cantilever. It thus allows the measurement of the interaction forces between the cell and a target surface in the so-called single-cell force spectroscopy (SCFS). Thanks to the acquired spatially resolved force curves, it is possible to get adhesion and mechanical maps of the cell surface with a high spatiotemporal resolution for bacteria of high medical importance [87,17, 89]. For example in the case of *S. aureus* cell, it was shown that intercellular adhesion is likely to originate from surface electrostatic interactions between cationic PIA (Polysaccharide Intercellular Adhesine) and teichoic acids [89]. Zn^{2+} strongly alters the structural, mechanical and adhesive properties of the cell surface, in that the surface morphology was much smoother, stiffer and stickier when this cation was present [90].

AFM experiments probed the adhesive interaction of Gram-negative *P. aeruginosa* T4P with hydrophobic surfaces [91]. From the observed constant force plateaus, it was proposed that these pili resist mechanical force by transitioning into an extended quaternary structure that may expose adhesive residues. Similar studies made on other Gram-negative strains revealed similar conclusions [80,75]. The pili mechanical properties in various Gram-positive bacteria were shown to be quite different [69,92]. *Caulobacter cresensus*, a Gram-negative,

divides asymmetrically and produces a swarmer cell and a sessile stalked cell. The stalked cell typically attach to a surface by a holdfast, an adhesive polar polysaccharide, found at the end of a thin elongated extension of the cell envelope, called a stack [93]. AFM measurements allowed the authors to monitor during the cell attachment the progressive growth of the newly secreted holdfast which strongly binds to surface and cures to form a plate-like glue capable of supporting strong and permanent adhesion. In another kind of study on *E. coli*, AFM measurements allowed the authors to study the relation between the self-association of adhesins and the rupture forces [94].

Direct quantification of detachment forces between bacteria and solid substrate was recently performed thanks to a new method combining the force control of an AFM with microfluidics: the cell was immobilized under physiological conditions on the pyramidal tip of a microchanneled AFM cantilever by underpressure. Forces of detachment of *Escherichia coli* from polydopamine substrate as an example were thus measured and studied for various conditions of contact time and applied force between cell and substrate [95].

When colonizing diverse surfaces, bacteria can also modify them via secretion of macromolecules. One of the defining characteristics of bacterial biofilms is the EPS matrix. Exopolysaccharide secreted by *P. aeruginosa* can work as a glue mediating early surface attachment [82,96,97].

Myxococcus xanthus surface motility has been recently studied using high-speed cell tracking and it was found that these cell trajectories consist of aperiodic stick–slip movements, driven by T4P-generated force acting against EPS-derived friction [98].

By using total internal reflection fluorescence microscopy (TIRFM) the gliding motility machinery of *M. xanthus* was recently analyzed. It was shown that it contains an inner-membrane motor complex that moves intracellularly along a right-handed helical path; when

the machinery becomes stationary at focal adhesion sites with the underlying surface, the motor complex powers a left-handed rotation of the cell around its long axis leading to the propulsion of the bacteria [99].

3. Mechanics of biofilms

While isolated bacteria swim in their environment they regularly meet various inert or living surfaces, onto which they can attach and initiate the development of a collective edifice by secreting multiple extracellular components, further gluing themselves to each other, leading to the creation of 3-dimensional biofilms. Local mechanics of isolated bacteria then becomes intimately integrated in the global mechanics of the whole biofilm edifice. Whereas the interplay between the two level on biofilm mechanics remains puzzling, several studies investigated mechanical aspects of biofilms: their viscoelasticity, heterogeneities and growth.

3.1. Viscoelasticity

Numerous rheological techniques (reviewed for instance in [10] or [12]) have been used at the macroscopic scale for the past two decades, which revealed biofilm viscoelastic behavior and occurrence of stress and strain in mechanically stimulated biofilms. In general the experiments are of two types: shear or compression tests. We present here some of the representative experiments, knowing that characterization technics are still under progress (see for instance [100]).

Both standard and specific rheometers with a given geometry (two parallel plates, cone/plate or Taylor-Couette) were used in static or oscillatory regime. As illustrated in Figure 4, rheometers impose either a stress (a force per unit area) or a strain (a deformation) by moving one plate and recording the resulting strain - or stress - respectively, which corresponds to

either creep or relaxation experiments. Uniaxial compression tests have been performed on biofilms compressed in a parallel plate rheometer [101-102]. The strain was imposed and the stress was measured. In [101], a hookean (elastic) solid zone in the stress versus strain curve was highlighted, corresponding to an apparent Young's modulus of 6.5 kPa. A relaxation experiment was conducted in [102] and different relaxation times were found. These times have been associated to bacterial rearrangements, water flows and extracellular matrix motions within the biofilm. In all cases, the biofilms can be either grown in situ (in a devoted rheometer, [103]), or ex situ and transferred subsequently [102,104].

In the typical creep experiment presented in Figure 4 A), the stress (top) is imposed and the strain measured (bottom). Basically the strain ε is equal to the stress σ_{shear} divided by the shear modulus G for an ideal elastic solid while for a liquid under loading, the strain varies linearly with time. The typical strain curve presented in Figure 4 A-bottom [12] clearly shows a combination of both behaviors and indicates that the biofilm has a viscoelastic behavior with long relaxation time (about ten minutes). In [105], very diverse biofilms, grown on one plate or directly transferred to the rheometer, were studied and the same type of curve was obtained in all cases. The authors found values of effective shear modulus ranging from 10^{-2} to 10^{6} Pa depending on the biofilm.

In another dynamical experiment (see Figure 4 B-top), the response to an oscillatory strain was measured. G' and G'' denote the storage and the loss moduli respectively. An ideal elastic solid material should respond with a constant G' value (non-nil) and a nil G'' value both being independent of the frequency ω. On the contrary the G'' response of a classical liquid should vary linearly with ω (the slope being proportional to the viscosity) and G' should be null. Here (in Fig. 4 B-bottom [103]) neither G' nor G'' is zero, and both vary with ω. These two observations indicate viscoelasticity. Moreover, as $G' > G''$ (about ten times

higher in agreement with [106]), the biofilms are viscoelastic solids rather than viscoelastic liquids and their variation with the frequency ω might be the signature of a system having different relaxation times, like polydisperse systems.

Many experiments have been carried out under liquid flow to renew the liquid composition during the biofilm formation. In these flow cells [107,108], the biofilm was subjected to a shear stress imposed by the flow. Changing the flow subjects then the biofilm to a hydrodynamic "load" usually defined by assuming the velocity profile in the flowing liquid. This allowed to monitor subsequent changes in the biofilm structure and to measure the strain experienced by the biofilm. Calculations of biofilm stiffness was therefore not direct and might need numerical integration [109] or the development of a model which predicts a fluid recirculation on the downstream side of the biofilm [110]. Recent progress of imaging methods also revealed the non-uniform structural deformation of the biofilm surface in contact with the liquid flow, together with the change of its internal porosity under loading and unloading [111]. The shear stress due to the flow changed the biofilm structure and removed protruding portions of biofilms, leading to flat and smooth biofilms [112]. It might also generate the formation of filamentous streamers [113,114,115]. Interestingly, analyzing the changes in filaments length while applying small increments in the flow rate, has enabled to estimate values of the apparent elastic modulus in the range of 70-140 Pa for filaments with a diameter around 5-20 μm [116], consistent with the typical values for macroscopic biofilms. Strong flow conditions might also produce rippled structures of the biofilm that were interpreted as a hydrodynamic instability [108,117].

Finally it can be mentioned that different studies have been also done on morphologies and mechanics of macroscopic biofilms standing at the air-liquid interface (termed pellicles), revealing the effects of molecular determinants on the structural, architectural and mechanical

properties [118,119]. Strain-hardening and viscoplastic effects were also observed in addition to viscoelasticity [120].

3.2. Heterogeneity

As broadly discussed in the literature, biofilms are so biologically and physico-chemically heterogeneous that generalization is challenging. Mechanisms contributing to the genetic and physiological heterogeneity within a biofilm population include microscale chemical gradients, adaptation to local environmental conditions, stochastic gene expression and some level of genotypic variations occurring through mutation. These mechanisms generate structural heterogeneities, gradients of growth rate and of stiffness among others as shown in the following [121]. Therefore biofilm behavior strongly depends on its composition in terms of bacterial species and on the culture conditions [122]. If millimeters size heterogeneity has been already reported when growing some biofilms on stained agar gel (Figure 5A) [123], other biofilms grown on top of liquid might be macroscopically homogeneous up to the meter scale [124].

A simple first striking observation when studying biofilm was that the thickness of a biofilm grown on a simple flat surface was highly non uniform [125]: areas covered by thick biofilms clusters reaching hundreds of micrometers of thickness juxtapose with areas partly covered or covered by thinner clusters. As shown in Figure 5B, a recent study has revealed the region-specific biofilm viscoelastic properties by means of particle-tracking microrheology [126]. This simple non-uniformity might be a first practical source of error when performing macroscopic measurements using two parallel plates for instance. Also the contact area of the biofilm to the plate, a value needed when converting force into stress, might change during indentation or compression.

When considering bacterial biofilm grown in a flow cell in continuous flow configuration, the top bacterial layers are in direct contact with liquid and have unlimited access to nutrients, whereas internal layers receive only what diffuses through the dense matrix. Similarly, in aerobic conditions, top layer bacteria are exposed to air, whereas the layers located inside biofilm depth develop in an increasingly anaerobic environment [127]. As a consequence of these gradients, the top layers are often constituted of fast growing cells, whereas biofilm bacteria grow more slowly in internal biofilm layers [128]. The slow growth rate of cells inside biofilms leads for instance to an enhanced tolerance to some antibiotics [129, 127].

As a consequence the biofilm mechanical behavior at the microscale is extremely diverse. As probed by magnetic micrometer-size beads, biofilms of *E. coli* (expressing surface appendages such as pili) behave either like a solid, a liquid or both at the bacterial scale (Figure 5 B&C)[130].

Further analysis of the local elastic and instantaneous compliance J_0 (inversely proportional to the instantaneous modulus; the higher the value the softer the domain) has been done in detail at different locations within a biofilm [130]. The authors observed dependence along the *z* distance from the substrate as illustrated in Figure 5D, and not along the other dimensions (over the 200 μm^2 explored area). Finally, they identified three vertically stratified layers: 1) a bottom layer of lowest compliance (highest rigidity) extending at 10-μm thickness close to the adhesive surface, 2) an intermediate layer of intermediate compliance extending over 20 micrometers and where the compliance distribution is very broad, which means that there is a coexistence of highly rigid and very soft areas, and 3) a soft top layer of 15-μm thickness in direct contact with the circulating liquid and where the compliance values may change with time by more than an order of magnitude from point to point [130]. In order to model the mechanical behavior of a biofilm attached to a solid substrate, some authors have more

recently suggested to incorporate heterogeneity into their model and consider the biofilm as a multi-layer composite material to explain their experimental results [131].

Finally composite effects have been also noticed when studying the deformation field of air-liquid interface biofilms (pellicles) [120]. Imaging the deformation of the biofilm structure followed by image analysis (using Particle Imaging Velocimetry program), the authors observed more pliable structures localized near attachment surfaces of the vertical container walls. These structures are less rigid than the center region, as they stretched more resulting in a non-affine deformation and in the need to correct the imposed strain to a true strain value.

3.3. Growth

If mechanical forces obviously play key roles in shaping living communities, current knowledge (characterization and understanding) on forces exerted between cells in multicellular environments are still limited [132]. For instance, to model the growth of a group of *E.coli* constituted of a small number of genetically and phenotypically identical bacteria that are not even organized in a biofilm, one has to consider repulsive forces between bacteria, frictional forces between neighboring bacteria, between bacteria and their substrates, and elastic forces exerted by the soft substrate on the bacteria when they grow in a confined environment. These forces act on the transition from two-dimensional growth to three-dimensional growth of micro-colonies and their magnitude may be actively tuned by the bacteria themselves. Once adhered to a substrate, bacteria may experience additional and non-trivial mechanical forces from the substrate as their protein synthesis may change depending on the substrate stiffness [133]. Cell clustering was for instance observed on soft substrates and not on rigid substrates suggesting that the mechanical forces between cells and substrates also mediate the interaction forces between dividing cells. An interesting recent study reveals how the asymmetric adhesion of cells increases cell-cell contacts [134].

The force dependence of the cell density is also far from being understood because of non-linear behaviors. Recent simulations and experiments indicate that disordered cell packings provided by microbial proliferation in a confined environment without any detected molecular connections between cells are stabilized by heterogeneous force networks where mechanical stress is mainly localized along branching "force chains" [135]. The resulting contact pressures were found high enough to slow down the cellular growth.

These recent findings point to the current lack of knowledge on the interplay between mechanical stress and growth in the bacterial communities and biofilms. However technical improvements and opening to other biophysics approaches helps to fill the knowledge gap. For instance optical imaging of biofilms with single-cell resolution recently revealed architectural transitions when isolated surface-attached bacteria multiply and secrete extracellular matrix during the biofilm growth [136]. When multiplying, *Vibrio cholerae* cells first remain in contact with the surface and then form a disordered 3D community which progressively evolves in a hedgehog-like structure with an anisotropic growth oriented perpendicular to the surface (the basal plane of attachment). These results suggest the presence of mechanical forces changing during the biofilm development, favoring a cellular ordered growth. Still, these forces remain to be elucidated.

Multicellular biofilm clusters have also been directly grown in chambers embedded with flexible micropillars where they may generate high enough forces (or "differential pressures") onto micropillars to deflect them [137]. Considering all the different studied bacterial strains, the authors reported differential pressure values ranging from 1 to 25 kPa. These values were strongly dependent on the matrix components as loss of some exopolysaccharides known for favoring lateral growth and spreading which reduces them by a factor of 2. It should be mentioned that pillars deflections of various amplitudes were also detected within the same

clusters. As discussed in the previous section and by Chew *et al.* [137], heterogeneity in growth and development of the clusters is an important distinctive feature of biofilm.

At a macroscopic scale, other studies succeeded in measuring the average force generated by the growth of *Bacillus subtilis* biofilms floating on top of liquid (pellicles) [124]. Using an original method and technics, the authors showed that this force comes from the biofilm growth at the air-liquid interface under the constraint that the liquid is contained in a dish of a finite size. This space restriction confines the pellicle while bacteria continue to multiply and secrete extracellular matrix; the growth under confinement induces a compressive force. The compressive macroscopic force was about -1 mN leading to a residual stress or a pre-stress of about -80 Pa and the pre-strain was found as high as -19%. Assuming an elastic behavior of the pellicle, it was possible to estimate a Poisson's ratio equal to 0.3-0.5 meaning a weakly compressive material with few exchanges of water molecules. Figure 6A illustrates a typical stress-strain curve recorded when elongating a piece of pellicle, grown *in situ* [120]. Because the pellicle is compressed by itself (by its growth), the force is negative without any applied strain, then decreases to zero and becomes positive during the elongation process. In absolute value, the magnitude of the initial growth compressive stress is as high as the magnitude of the tensile stress measured after 20% of elongation. This result shows how important it is to perform the mechanical experiments *in situ* and to define the pre-stress level of the initial state. In addition the experiments indicated an elastic behavior in the compression range at small deformations and a viscoplastic behavior in the tension range at large deformations.

Experiments have shown that this force, associated to a growth-pressure, relaxes over very short time scales (tens of milliseconds) [124] while biofilm relaxation upon loading is very long, typically few minutes or tens of minutes as commonly observed [105]. This force spontaneously spreads the biofilm towards free surrounding spaces and may cover any small holes that could appear within the structure [124]. Therefore, it facilitates self-healing and

contributes to maintain the biofilm integrity. This effect may be compared to the self-healing effect observed in hydrogels and discussed in the paragraph 4.2. Another important feature that might be mentioned concerns the relaxed state. When deformed after loading, the pellicle slowly relaxes back towards a compressed state and not to a zero-stress state. This effect is likely due to the innate arrangement of the pellicle structure as it formed under compression during growth [120].

Many pellicles at the air-liquid interface exhibit wrinkles and folds during their maturation process, which are considered as a distinctive morphological phenotype. Their presence was interpreted as the result of the compressive force (pre-stress) [138]. The authors have explained the wrinkle formation using the buckling mechanical instability applied to an elastic sheet floating on top of a liquid and found good agreement between the wavelength predicted by the buckling model and the observed wavelength. Part of a large pellicle which starts to buckle is illustrated in Figure 6B (top view). A maze-like pattern of wrinkles can be observed on the down side of the Figure and is due to the 2D compressive pre-stress when the pellicle is confined along its two axes. The blue arrows indicate the presence of 2D compressive forces. By cutting and removing parts of the pellicle on its lateral sides, the confinement was suppressed along one axis. As a result, the wrinkles symmetry has changed and they lined up in one direction under the effect of a 1D compressive force. This experiment shows also how elastic is the pellicle when it starts to wrinkle as the wrinkles are able to reorient according to the geometrical constraints.

Biofilms grown on agar gel (solid elastic substrate) have also rich and complex 3D architectures exhibiting wrinkles and folds (Figure 7A). Some patterns published in the literature are rearranged in Figure 7. Unlike pellicles grown under the constrained boundaries condition, these biofilms are not limited spatially by lateral boundaries. Experiments revealed the presence of death cells (Figure 7B), of channel networks, spatial and temporal differences

in matrix production and composition [139,140,141]. All these heterogeneities combined with an interaction with the substrate contribute to generate stiffness gradients, differential/anisotropic growth and to favor the presence of mechanical stresses within the biofilm (Figure 7C and D). Few theoretical attempts have been proposed to explain the different patterns [142,143,144], by combining the buckling mechanical instability with the biofilm elasticity and the biofilm growth (see section 4.2 for a discussion on the growth modeling).

4. Comparison with other systems

As shown in Parts 2.1 & 2.2, the cell wall envelope mostly contributes to the bacterial stiffness with typical elastic moduli ranging from 10 kPa to few MPa, 10^5 Pa being the order of magnitude commonly reported in the literature. We can therefore consider bacteria as 10 to 1000 times stiffer than biofilms. Although the biofilm architecture is regulated by the biological activity of bacteria, the biofilm environment might be compared to a hydrogel enriched by rigid colloids as recalled by Mazza in a recent review [9].

Extracellular Matrix (ECM) can account for up to 90% of the biofilm dry mass [145], indicating that about 10% of rigid cell composes the biofilm which is the typical fraction of colloids found in hydrogels as discussed later in Part 4.1. The matrix itself includes polysaccharides, proteins, DNA, lipids, and cell lysis products; it is described by the abbreviation EPS standing for Extracellular Polymeric Substances rather than ECM, showing how important is the polymer notion for biofilm constituents. Biofilm polysaccharides (cellulose, ß-1-4 N acetyl glucosamine polymers etc.) are often very large polymers and proteins may form long fibers too. Local organization of the components within the biofilms is not well-documented, due probably to its variability and the difficulty of measuring it

experimentally without perturbation and to be extremely various. Berk *et al.* reported the existence of dynamic and flexible envelopes encasing cell clusters composed by polysaccharides and several proteins [146].

The EPS organization could therefore be considered in a first approach as disordered and heterogeneous within the same biofilm and with multiple connections between the different components (see Part 3.2). We may envision the biofilm as a multiple network of various elastic and rigid links swollen by about 60 % of water (a typical fraction commonly reported in the literature).

Because of the numerous similarities between biofilms and non-biological synthetic hydrogels, we present in the next paragraph a brief review on hydrogels from the classical notion of swelling to the most updated studies on self-healing; all these concepts are relevant to biofilm studies. Moreover, if biofilms appear or behave like hydrogels, they share common features with other of other multicellular systems such as living tissues: they are active, they grow and secrete extracellular matrix and we will present a short review on the mechanics of living tissues. Finally Young's moduli of some living tissues, hydrogels and biofilms are reported in Table 2.

4.1. Hydrogels enriched with colloids

A hydrogel can be defined as a network of flexible polymer chains that can contain a large amount of water, typically 60-90 wt % like in many biofilms. Although the material is mostly water-based, the gel behaves like an elastic solid as cross-links maintain the topology of the polymer network on a long time-scale with respect to the duration of the observation. Gels are defined as *chemical gels* or *physical gels* depending on the nature of the cross-links between polymer chains, i.e. permanent covalent bonds or reversible interactions. Gels act

simultaneously as macromolecular reservoirs and exhibit analogies with solutions or dialysis bags wherein the soluble molecules can diffuse and be outsourced from the network.

By analogy to the biofilms case, it's interesting to focus on the conditions of polymeric gel synthesis and the definition of the preparation state before reviewing the actual route for gel reinforcement involving multiple networks and nanocomposites.

4.1.1. Synthesis, frozen inhomogeneities and swelling

A gel is a frozen system. Although the dynamics of the polymer chains are dominated by thermal fluctuations, network topology is set during synthesis. Whatever the polymerization route is : from monomers or by end-chain reactions, with or without solvent, the gelation process leads to frozen inhomogeneities in the system. This complex process has been theoretically investigated [147,148,149] with the support of experimental techniques such as neutron scattering [150,151] or light scattering [152]. Cross-linking inhomogeneities play a crucial role in the mechanical response of the network, especially in terms of strain hardening or damage initiation as it has been demonstrated for 'dried gels' (i.e. cross-linked elastomers) [153,154], but such inhomogeneities are even more exacerbated when the network is highly swollen by a solvent [155].

The control of the network architecture is extremely difficult to achieve. Parameters such as the initial monomer or polymer concentration, the temperature, the solvent quality, the yield of polymerization, or the polymerization kinetics will define the network topology. To understand the network properties, two aspects need to be considered: i/ the conditions of network formation, defined as the preparation state and ii/ the situation at the moment of the study. However, gels are often only defined by their polymer volume fraction ϕ_p during their characterization, or equivalently by their swelling degree Q defined as $Q = 1/\phi_p$. If the swelling degree Q provides the gel composition, it does not reflect the network state with

respect to the conditions of network formation. Indeed, by defining the preparation conditions as initial swelling degree (denoted as Q_0) independently from the maximum swelling conditions in water (or solvent) referring to the swelling equilibrium Q_e, a given gel studied at an intermediate condition of hydration Q_i undergoes an elongation λ of the same intensity in all three directions of space with $\lambda = (Q_i/Q_0)^{1/3}$. Starting from the classical theory of rubber elasticity [156,157,158], elastic modulus of a dried rubbery network directly derives from the number of elastically active chains of the network per unit of volume times the thermal noise (of energy *kT*). Panyukov *et al.* [149] and Rubinstein et al. [159] have proposed elasticity models that refine the concept to gels and take into account the swelling ratio (relative to the initial swelling) but also the conditions of the chain solvability in the water (or solvent). Thus, the elasticity of the polymer network is not just a function of the volume fraction of polymer, nor *kT* times the number of elastically active chains in the gel, but the elasticity will vary more subtly on the interactions at play between polymer and solvent.

When immersed in an excess of appropriate solvent, gels can often swell considerably. The swelling is driven by the favorable free energy of mixing with solvent (osmotic pressure, π) and is resisted by the energy required to stretch the network strands (elastic modulus, *G*). The gel swells up to the equilibrium state when the osmotic and the elastic parts of the free energy counterbalance, i.e. when $G \cong \pi$.

The notions of swelling up to a state restricted by the elasticity of the network and of equilibrated pressures inside and outside the gel apply in the case of bacteria and biofilms. At a bacterium scale, cells which are embedded within the biofilm may experience a major increase in extracellular osmotic pressure due to the presence of extracellular polymeric network. They are also subjected to an osmotic regulation from inside to outside their body partly through interplay between mechanical tension of the cell wall and mecano-sensitivity

of the channels (see Part 2). To prevent the loss of cellular water, cells in response accumulate osmoprotectant molecules [160,161,162]. At the biofilm scale, Seminara *et al.* [163] have already proposed a model to explain how the biofilm spreading is facilitated by the secretion of matrix when growing on an agar gel: the EPS secretion induces locally an osmotic pressure gradient which forces water to flow from the agar gel to the biofilm in order to equilibrate the pressure.

Biofilm growth and gel swelling generate a local volumetric increase of the elastic material. If the notion of osmotic equilibrium applies as a driving force for water flow, the gel swelling may induce mechanical instabilities in the case of osmotic gradients. As illustrated in Figure 8, the elastic modulus of a gel decreases when absorbing water leading to internal stiffness gradient and subsequent morphological instabilities, similar to the ones described in Figure 7. These mechanical instabilities depend on water diffusion and vanish once the osmotic equilibrium is reached without any more gradients. Hence a spherical and hydrophilic hydrogel immersed into water expands progressively by following a series of morphologic changes until becoming spherical again after several hours [164,165]. The gel experiences temporarily local internal stress during the swelling. Similar instability occurs when swelling a strip of soft gel attached to a rigid gel [166]; the flat state becomes unstable above a critical swelling rate. See for instance two reviews on mechanical instabilities in gel and soft materials in References [167,168].

4.1.2. Routes for gel reinforcement and gluing: macromolecular design

It’s informative to compare the mechanical response of biofilms and of chemical gels and to review which routes are considered nowadays for gel reinforcement. As shown in Part 3, biofilm stiffness strongly depends on species, bacterial strain or on culture conditions. On one hand, biofilms have to be strong enough to withstand external flux or mechanical loading

allowing them to grow and proliferate. On the other hand, heterogeneities favour the detachment of some biofilm fragments which allow dissemination and colonization of other spaces. In the case of synthetic hydrogels, used in many industrial applications as soft materials, many efforts have been devoted during the last two decades, to overcome gels fragility by exploring a wide richness of macromolecular topologies ([169,170] and references herein). Figure 9 illustrates some pioneered approaches.

The reduction of the cross-link inhomogeneities is one efficient option that has been developed by Ito *et al.* [171] with sliding-ring cross-linked gels (Figure 9 (a)) and Sakai *et al.* [172] with tetrahedron-like macromonomers gels (Figure 9(b)) that allow for well-controlled chain length distribution between chemical cross-links. Such types of architecture permit an optimal cooperativeness of the polymer strands of the network that retards damage initiation. But, after exhaustion of the conformational changes of the network chains, fracture propagates readily without contribution of other dissipative mechanisms [173]. Other groups have explored other routes with the aim of promoting dissipative processes to enhance efficiently fracture toughness. For instance, Gong and co-workers pioneered the idea of introducing mechanical dissipation in chemically cross-linked gels by introducing sacrificial covalent bonds. As shown in Figure 9 (c), authors developed double network (DN) gels [174] which result from the synthesis of a primary highly cross-linked and a highly swollen network with a secondary network loosely cross-linked, and entangled with the primary network [175]. By sacrificing the integrity of the brittle primary network, the second network ensures the stress transfer and enlarges the damage zone before catastrophic fracture occurs. A subtle control of gel formulation (by using different monomers or polymers, by adjusting cross-linking concentrations and swelling state, by controlling gelation conditions, etc.) enables dramatic improvements of the fracture toughness: tearing fracture energies were reported to be as high as 1000 J m^{-2} (same order of magnitude of unfilled rubber tearing energy) [176].

Note that if this concept enables a tremendous increase of dissipation by bond-breaking, after being operated, the macromolecular architecture is permanently damaged without any chance of recovery. Nevertheless, DN gels have other valuable mechanical properties related on their intrinsic covalent nature, such as low sliding friction, good wear resistance, good fatigue resistance that make DN gels good candidates for in vivo applications [177]. The DN concept has been directly applied to elastomers [178] or by introducing reversible cross-links [179].

In contrast to DN gels which imply a fine control of chemistry, Haraguchi and co-workers [180] polymerized linear chains (without chemical cross-links) in the presence of clay nano-platelets and developed the first highly extensible nanocomposite gels (NC gels). First results [181,182] demonstrated very interesting mechanical properties: NC gels featured very high deformability (up to 1000%) and adjustment of gel stiffness was achieved simply by varying the clay concentration without sacrificing extensibility too much. Authors envisaged polymer chains to be grafted onto neighbouring clay platelets by emphasizing the importance of initiating the polymerization from the clay surface and underlining the fact that by introducing a chemical cross-linker together with inorganic clay, gels became very brittle. This work opened the field for NC gels studies [183,184,185]. A more comprehensive picture of the mechanisms of NC gel reinforcement was obtained by using model hybrid networks [186,187], i.e. using silica nanoparticles (NPs) to ensure a good dispersion state and avoid complex effect of alignment upon mechanical stretching that make more complex mechanistic interpretations [188]. As shown in Figure 10, the principle relied on using polymer adsorption on nanoparticles (NPs) to design reversible sacrificial bonds while chemical cross-links permanently fix the network topology. Hybrid gels exhibited a remarkable combination of properties: initial modulus, strength at failure and stretchability were seen to be simultaneously enhanced by increasing the NP volume fraction.

Silica NPs enabled topological rearrangements within a characteristic time-scale. Thus, within the appropriated frequency domain, local rearrangements and exchanges between adsorbed and desorbed states allowed for stress relaxation of the polymer network and retarded efficiently fracture processes. Interestingly full recovery, in terms of mechanical behaviour and residual strain, was achieved after tens of seconds at rest. Within this time-scale, the network is able to self-reorganize (self-heal in bulk) in order to recover an equivalent network. This concept opened up a simple method for gel adhesion using NP solutions as a glue [189]. This method is very versatile since polymers are very prone to adsorb onto solid surfaces. Thus, it has been demonstrated that it is possible to glue gels of different chemical natures and the adhesion remains when the joint is immersed in water and swells. The promise of the method was illustrated for biological tissues [190].

In this context, biofilm complex organization involves a multiple network combining various polymeric and proteinaceous links with rigid bacteria and it may share common features with the most recent hybrid gels. It is difficult to check whether an increasing fraction of bacteria passively enhanced initial modulus, strength at failure and stretchability but it is known that some biofilms present a large distribution of relaxation times which implies multiple rearrangements within the structure. Note that the biofilm network is able to self-organize in several ways: simply by growing which takes time to remodel the network, or by rapidly relaxing the residual stress as shown on biofilms floating on top of liquid [124]. Lieleg *et al.* also reported a recovery of biofilm stiffness few minutes after yielding [106].

Another common feature between biofilms and the hybrid gels remains their stickiness. Gluing different gels by particles is also interesting in the context of biofilm as biofilms are well-known for their stickiness [4]. If adhesive forces mediated by the matrix have been reported at the bacterium scale (see Part 2.5.), it’s well-known that biofilms strongly adhere to mostly any substrates and are difficult to remove once a surface has been colonized.

4.2. Living tissues

Biofilms do not have equivalent in non-unicellular organism. Still, they share some similarities with soft collagen-rich tissues (or connective tissues), as tendon, dermis or aorta: they are formed of single cells embedded in a soft matrix [191], and they can grow in time.

These tissues are also made of extra-cellular matrix (ECM), which is secreted by the eukaryotic cells in the tissues, but the composition is completely different. While biofilms are mostly polymer-like structure, ECM is formed by a mixture of fibrillary proteins (collagen and elastin), embedded in soft, disorganized, matrix of biomolecules and water [192,193]. The differences between the connective tissues are often viewed as differences in the architecture of these different elements [194,195,196]: in tendon, the fibers are aligned, while in skin, fibers are disorganized (see Figure 11). Still, all the soft collagen-rich tissues are close in term of mechanical properties [197,198,199,200,201]: they support large stretches, are anisotropic, have a viscoelastic response and the so-called "preconditioning" effect. Preconditioning is related to the Mullin's effect: when a tissue is repeatedly loaded at the same level (either in stretch or stress), the stress-stretch response will slowly shift toward a limit cycle as the microstructure reconfigures [202,203]. In that sense, they are similar to biofilms, despite a completely different stress-stretch response.

As shown in Figure 12, the soft tissue behavior is generally described as a three-phase response [199,204]. First, we have the toe region, in which the tissue supports large stretches with low forces. Second, the heel region is associated with a non-linear increase of the force with the stretch. Finally, in the linear region, the force is proportional to the stretch. These three regions are classically associated to the collagen-fibers response (Figure 12): in the toe region, the fibers are crimped and the force comes from the non-fibrillar matrix; in the heel region, the fibers are aligning toward the direction of traction, and the linear is then due to the

stretching of the fibers. In the first stretching, a sliding between collagen fibers is also observed [205], which implies a reconfiguration of the network and may explain the preconditioning [202]. This microstructural interpretation of the stress-stretch curve has been well established in tendon [202,205,206,207], while being still under debate for other tissues [208,209].

Despite their differences in behavior, and in their microstructural origin, the formalism used to describe the soft collagen-rich tissues and the biofilms are close. To describe the behavior at large stretch, a hyperelastic description based on an invariant-based energy [194,199,210,211] is commonly used. Visco-elasticity is also often introduced to describe either the strain rate dependency [212] or the preconditioning [213].

Apart from pure material considerations, biofilms and soft tissues shared the same living ability to grow. Growth is, in fact, found in most living complex tissues, as pointed in the more complete review by Jones and Chapman [214]. Growth is associated with an increase of the mass of the system – and then often to its volume. When the growth occurs in a confined environment, elastic tissues adapt by deforming themselves. This may push on the external obstacles [124,215]; for non-homogeneous growths or growths in a confined environment, it may also induce residual stretches and stresses [194,216]. Residual stresses are self-balanced, meaning that they exist inside of the tissue, even without external force being applied. Perturbations, as cuts, of the tissue may relax these stresses, inducing significant deformations. Wood provides a spectacular example: the growth of the tree, especially in a windy and tilted environment, can create large stresses inside the plant. These stresses are problematic since the trunk may crack when sawed, losing most of its value as illustrated in Figure 13 [214]. This crack opening is due to the tension in the trunk. Confined growth more often lead to compressive stresses (associated to a positive pressure in the tissue), the growing material pushing against the surrounding medium. This can induce shape instabilities, as

observed in swelling gels (in Fig. 8). Releasing the confinement leads to a rapid expansion of the material. This could favor the propagation of cancer cells if a tumor is cut during its surgical ablation [215]. On the contrary, it prevents the formation of holes when the tissue remains confined, explaining partly the robustness of biofilms to mechanical attacks. Two main experimental difficulties are faced to determine the residual stresses. First, it is released only when a hole is created in the material, which may be a problem while studying living systems. Second, the observation is in fact the opening of the hole, which relates to the strain and not to the stretch. In that sense, the biofilm case is interesting by its simplicity and robustness. Indeed, it is possible to make the biofilm growth in a confined environment equipped to measure the load, and thus to measure directly the residual stresses and its evolution in time [124].

For an elastic material, as biofilms and most soft tissues, the theoretical frame to model the growth is now well established since Rodriguez et al. [217]. The core difficulty was that the growth creates new material in a state which is not known. Thus, the main idea is to start from a reference, stress-free, state – which does not have to be visible in the experiment. Then the problem is split into two steps: first, the growth, and then the elastic response (see Figure 14). The growth does not have to create a compatible solution: it can contain holes, material points can be at the same position and the solid doesn't have to respect the boundary condition. The associated tensor is thus purely given by biological considerations on the evolution of the mass distribution between the "reference" and current configurations. Then, the elastic response corrects all these incompatibilities and create a mechanically compatible state. Due to its simplicity and its generality, this frame has been applied to a large range of problems, from the aorta [218,194] to skin [219], through brain [220], as well as many other ones [221,222,223].

Despite the elegance and the simplicity of this formalism, some difficulties remain. The first one is to determine the proper "stress-free" reference configuration. A second question, deeply related, is the choice of the growth. Indeed, it is not possible, for a given shape, to distinguish what is due to the growth and what is due to the elastic response, without mechanical assays. Two main approaches are used to tackle these problems. The first one focusses on the stability of a chosen initial shape: starting from a sphere or a cylinder and introducing different growth magnitude and distribution inspired by biological consideration, one can analyze the limit of stability of the initial shape, and what will be the pattern in the tissue [224]. A second approach focusses on the growth of existing tissues – as for example the growth of tumors [221] or the extension of skins for graft [225]; the initial configuration is then given by the shape of the tissue before its growth.

The main limit of this formalism is to impose the growth as a whole process, independently of the history of the system. In fact, in many cases, the growth rate is affected by the stress on the cells [226]. To avoid this difficulty, the natural option will be to use the same approach incrementally [227]: first make the tissue growth, second compute the stress, and then determine the new growth and so on. However, this approach is time-consuming, and in some cases as the growth of aneurysm, it can be avoided by assuming that the stress state of the new material is determined and related to the current stress [228].

This short review on growth modeling has to be concluded with few words on other approaches: we presented the macroscopic description of the growth of a purely elastic material. It is therefore perfectly adequate for biofilms in a first approach, but not relevant for other situation. Some growth processes are well described with simpler models, as for example the uniaxial growth of plants [229]. Some materials are not elastic but mostly fluid: the growth is then viewed as a source term in the fluid [230,231]. Also, in many cases, we are

interested in a local description of the growth – especially for cellular tissues – which includes the details at the cell scales. Then a discrete model may be relevant [232].

5. Conclusions

Whereas numerous mechanical studies focused on stiffness and viscoelasticity of bacteria and biofilms, and considered these systems as quasi-static materials, recent works point to the need of understanding the role played by growth and heterogeneities on their mechanical properties. Both phenomena can generate mechanical instabilities at the level of single bacterium as well as at a macroscopic scale. We discussed how these instabilities may help bacteria to divide by propagating a mechanical crack or biofilm communities to keep growing by shaping wrinkles and folds. Little is known about the presence of residual mechanical forces and their potential role on the bacteria metabolism. Bacteria embedded in biofilm might be sensitive to their mechanical environment. It would be interesting to understand how they are able to secrete extracellular matrix while subjected to a confined space or while being subject to the compression exerted by other bacteria or exerted by a surrounding extracellular matrix.

Little is also knownon the bacterial behavior in a heterogeneous mechanical environment, for instance how single cells grow or produce ECM in an environment having a stiffness gradient. They might grow in the direction of minimal mechanical resistance which would mean that the stiffness gradient acts like a nutriment or oxygen gradient and directs the growth. Although the exopolysaccharide export from a cell doesn't seem to directly involve mechanosensitive components [233], we might wonder which effects on cell metabolism and on active polymerization and secretion process could have a heterogeneous mechanical environment. Would it change the spatial distribution along the cell of the secreting components like the protein channels or simply modify their biosynthesis activity?

Mechanical cues may appear therefore as a counterpart to the chemical cues and their identifications constitute a promising direction for understanding bacteria and biofilms behaviors.

Comparison between the different systems of chemical or biological synthesis shows also the difficulty to define a mechanical reference state when modeling the systems. Chemical gels are frozen states with a topology set during the synthesis; the reference state corresponds to the preparation state incorporating frozen heterogeneities and subsequent residual stresses. Living systems grow, generating a pre-stress (the residual stresses); the reference state corresponds to a free-stress state difficult to determine as being unreal and as the growth often depends on the tissue history.

Recovery, self-healing, self-repairing and stickiness are also important features common to biofilms and hybrid hydrogels requiring facilitated and dynamic rearrangements of the networks. If biofilm architecture and dynamics may inspire the generation of future hybrid gels, in turn understanding the properties of well-controlled gels may help understand the multiple behaviors of biofilms.

Aknowledgements

Eric Raspaud and Jean-Marc Ghigo would like to thank the CNRS for funding the emerging project “BIOFFORCE” (Défi Instrumentation aux limites, 2015). This work is supported by “Investissements d’Avenir” LabEx PALM (ANR-10-LABX-0039-PALM) that Christian Marlière and Eric Raspaud would like to thank. Jean-Marc Ghigo is supported by grants from the French Government's Investissement d'Avenir program, Laboratoire d'Excellence "Integrative Biology of Emerging Infectious Diseases" (grant n°ANR-10-LABX-62-IBEID). Alba Marcellan acknowledges Ph.D. fellowship fundings from ED397, UPMC, Paris France;

the financial support of the CNRS, the ESPCI and the UPMC is acknowledged. The authors would like to thank Christophe Beloin for his critical reading and his stimulating comments. Finally Eric Raspaud would like to thank the co-editors and Dominique Langevin for the invitation.

Références

[1] Lopez HM, Gachelin J, Douarche C, Auradou H, Clement E, Phys Rev Lett, 2015; 115(2): 028301.
[2] Doostmohammadi A, Thampi SP, Yeomans JM, Phys Rev Lett, 2016; 117 (4): 048102.
[3] Wilking JN, Angelini TE, Seminara A, Brenner MP, Weitz DA, MRS Bull, 2011; 36: 385.
[4] Pamp SJ, Gjermansen M, and Tolker-Nielsen T. In Kjelleberg S, Givskov M (editors), The Biofilm Mode of Life: Mechanisms and Adaptations. Norfolk, UK, Horizon Bioscience; 2007. p. 37.
[5] Branda SS, Vik A, Friedman L, Kolter R, Trends Microbiol, 2005; 13(1): 20.
[6] Sanchez-Vizuete P, Le Coq D, Bridier A, Herry JM, Aymerich S, Briandet R, Appl Environ Microbiol, 2015; 81(1):109.
[7] May T, Okabe S, J Bacteriol, 2008; 190(22): 7479.
[8] Persat A, Nadell CD, Kim MK, Ingremeau F, Siryaporn A, Drescher K, Wingreen NS, Bassler BL, Gitai Z, Stone HA, Cell, 2015; 161(5): 988.
[9] Mazza MG, J Phys D : Appl Phys, 2016; 49: 203001.
[10] Head D, Springer International Publishing Switzerland 2016; MC Leake (ed.), Biophysics of infection, Advances in experimental medicine and biology 915: 99.
[11] Lecuyer S, Stocker R, Rusconi R, New J Phys, 2015; 17: 030401.
[12] Guélon T, Mathias JD, Stoodley P, Springer-Verlag Berlin Heidelberg 2011; HC Flemming et al (eds), Biofilm Highlights, Springer Series on Biofilms 5: 111.
[13] Clement E, Lindner A, Douarche C, Auradou H, Eur Phys J Special Topics, 2016; 225:2389-2406.
[14] http://iopscience.iop.org/journal/1367-2630/page/Focus%20on%20Bacterial%20Mechanics;jsessionid=76F73D7A512E1A40B99018E200ADB0C2.c4.iopscience.cld.iop.org
[15] Aguayo S, Bozec L, Adv Exp Med Biol, 2016; 915: 245–260.
[16] Chen Y, Norde W, Mei HC, van der Busscher H J, mBio, 2012; 3 (6): e00378-12.
[17] Dufrêne YF, mBio, 2014; 5 (4): e01363-01314.
[18] Dhahri S, Ramonda M, Marlière C, PLoS ONE, 2013; 8 (4): e61663.
[19] Formosa C, Grare M, Duval RE, Dague E, Nanomedicine Nanotechnol Biol Med, 2012; 8 (1): 12–16.
[20]Wu Y, Zhou A, Chem Commun, 2009; 45: 7021–7023.
[21] Aguayo S, Strange A, Gadegaard N, Dalby M J, Bozec L, RSC Adv, 2016; 6 (92): 89347–89355.
[22] Pelling AE, Li Y, Shi W, Gimzewski JK, Proc Natl Acad Sci USA, 2005; 102 (18): 6484.
[23] Francius G, Polyakov P, Merlin J, Abe Y, Ghigo J-M, Merlin C, Beloin C, Duval JFL, PLoS ONE, 2011; 6 (5): e20066.
[24] Mularski A, Wilksch J, Hanssen E, Li J, Tomita T, Pidot SJ, Stinear T, Separovic F, Strugnell DA, Eur Biophys J EBJ, 2016.
[25] Dombrowski C, Kan W, Motaleb MA, Charon NW, Goldstein RE, Wolgemuth CW, Biophys J, 2009; 96 (11): 4409–4417.
[26] Caspi Y, PLOS ONE, 2014; 9 (1): e83775.
[27] Sun X, Weinlandt WD, Patel H, Wu M, Hernandez CJ, Lab Chip, 2014; 14 (14): 2491–2498.
[28] Höltje J-V, Microbiol Mol Biol Rev, 1998; 62(1): 181–203.
[29] Turner RD, Vollmer W, Foster SJ, Mol Microbiol, 2014; 91 (5): 862–874.

[30] Daly KE, Huang KC, Wingreen NS, Mukhopadhyay R, Phys Rev E, 2011; 83 (4): 041922.
[31] Scott Cayley D, Guttman HJ, Thomas Record Jr M, Biophys J, 2000; 78 (4): 1748–1764.
[32] Dover RS, Bitler A, Shimoni E, Trieu-Cuot P, Shai Y, Nat Commun, 2015; 6: 7193.
[33] Liu TT, Lin YH, Hung CS, Liu TJ, Chen Y, Huang YC, Tsai TH, Wang HH, Wang DW, Wang JK, et al., PLOS ONE, 2009; 4 (5): e5470.
[34] Errington J, Nat Rev Microbiol, 2015; 13 (4): 241–248.
[35] Rojas E, Theriot JA, Huang KC, Proc Natl Acad Sci USA, 2014; 111 (21): 7807–7812.
[36] Nguyen LT, Gumbart JC, Beeby M, Jensen GJ, Proc Natl Acad Sci USA, 2015; 112 (28): E3689–E3698.
[37] Wachi M, Doi M, Tamaki S, Park W, Nakajima-Iijima S, Matsuhashi M, J Bacteriol, 1987; 169 (11): 4935–4940.
[38] Jones LJ, Carballido-López R, Errington J, Cell, 2001; 104 (6): 913–922.
[39] Daniel RA, Errington J, Cell, 2003; 113 (6): 767–776.
[40] Garner EC, Bernard R, Wang W, Zhuang X, Rudner DZ, Mitchison T, Science, 2011; 333 (6039): 222–225.
[41] Domínguez-Escobar J, Chastanet A, Crevenna AH, Fromion V, Wedlich-Söldner R, Carballido-López R, Science, 2011; 333 (6039): 225–228.
[42] van Teeffelen S, Wang S, Furchtgott L, Huang KC, Wingreen NS, Shaevitz JW, Gitai Z, Proc Natl Acad Sci USA, 2011; 108 (38): 15822–15827.
[43] Boulbitch A, J. Electron Microsc (Tokyo), 2000; 49 (3): 459–462.
[44] Thwaites J, Mendelson N, Int J Biol Macromol, 1989; 11 (4): 201–206.
[45] Mendelson N, Thwaites J, J Bacteriol, 1989; 171 (2): 1055–1062.
[46] Deng Y, Sun M, Shaevitz JW, Phys Rev Lett, 2011; 107 (15): 158101–1_4.
[47] Zhou X, Halladin DK, Rojas ER, Koslover EF, Lee TK, Huang KC, Theriot JA, Science, 2015; 348 (6234): 574-578.
[48] Hamill OP, Martinac B, Physiol Rev (2001); 81(2): 685-740.
[49] Booth IR, Curr Opin Microbiol, 2014; 18: 16–22.
[50] Kung C, Nature, 2005; 436 (7051): 647–654.
[51] Booth IR, Cairney J, Sutherland L, Higgin CF, Soc Appl Bacteriol Symp Ser, 1988; 17: 35S–49S.
[52] Reuter M, Hayward NJ, Black SS, Miller S, Dryden DTF, Booth IR, J R Soc Interface, 2014; 11 (91): 20130850.
[53] Peyronnet R, Tran D, Girault T, Frachisse JM, Front Plant Sci, 2014; 5(558): 1-14.
[54] Evans E, Ludwig F, J Phys Condens Matter, 2000; 12: A315.
[55] Boer M, Anishkin A, Sukharev S, Biochemistry, 2011; 50: 4087-4096.
[56] Yao X, Jericho M, Pink D, Beveridge T, J Bacteriol, 1999; 181 (22): 6865–6875.
[57] Pilizota T, Shaevitz JW, Biophys J 2013; 104 (12): 2733–2742.
[58] Pilizota T, Shaevitz JW, PLOS ONE, 2012; 7 (4): e35205.
[59] Zakrisson J, Singh B, Svenmarker P, Wiklund K, Zhang H, Hakobyan S, Ramstedt M, Andersson M., Langmuir, 2016; 32 (18): 4521–4529.
[60] Nan B, Zusman DR, Mol Microbiol, 2016; 101 (2): 186–193.
[61] Craig L, Pique ME, Tainer JA, Nat Rev Microbiol, 2004; 2 (5): 363–378.
[62] Shrout JD, Trends Microbiol, 2015; 23 (5): 244–246.
[63] Andersson M, Björnham O, Svantesson M, Badahdah A, Uhlin BE, Bullitt EA, J Mol Biol, 2012; 415 (5): 918–928.
[64]Chahales P, Thanassi DG, Microbiol Spectr, 2015; 3(5): UTI-0018-2013.
[65] McWilliams BD, Torres AG, Microbiol Spectr, 2014; 2(3): EHEC-0003-2013.
[66] Korea CG, Ghigo JM, Beloin C, Bioessays, 2011; 33(4): 300-311.

[67] Madhavan TPV, Sakellaris H, Adv Appl Micro, 2015; 90: 155-197.
[68] Li Y-F, Poole S, Nishio K, Jang K, Rasulova F, McVeigh A, Savarino SJ, Xia D, Bullitt E, Proc Natl Acad Sci USA, 2009; 106 (26): 10793–10798.
[69] Tripathi P, Beaussart A, Alsteens D, Dupres V, Claes I, von Ossowski I, de Vos WM, Palva A, Lebeer S, Vanderleyden J, et al. ACS Nano, 2013; 7 (4): 3685–3697.
[70] Hahn E, Wild P, Hermanns U, Sebbel P, Glockshuber R, Häner M, Taschner N, Burkhard P, Aebi U, Müller SA, J Mol Biol, 2002; 323 (5): 845–857.
[71] Mortezaei N, Singh B, Zakrisson J, Bullitt E, Andersson M, Biophys J, 2015; 109 (1), 49–56.
[72] Andersson M, Fällman E, Uhlin BE, Axner O, Biophys J, 2006; 90 (5); 1521-1534.
[73] Andersson M, Fällman E, Uhlin BE, Axner O, Biophys J, 2006; 91 (7): 2717–2725.
[74] Thomas WE, Nilsson LM, Forero M, Sokurenko EV, Vogel V, Mol Microbiol, 2004; 53(5):1545-1557.
[75] Miller E, Garcia T, Hultgren S, Oberhauser AF, Biophys J, 2006; 91(10); 3848-3856.
[76] Zakrisson J, Wiklund K, Servin M, Axner O, Lacoursière C, Andersson M, Eur Biophys J, 2015; 44 (5): 291–300.
[77] Jacquot A, Sakamoto C, Razafitianamaharavo A, Caillet C, Merlin J, Fahs A, Ghigo JM, Beloin C, Duval JFL, Francius G, J Biomed Nanotech, 2014; 10: 3361-3372.
[78] Castelain M, Ehlers S, Klinth J, Lindberg S, Andersson M, Uhlin BE, Axner O, Eur. Biophys J, 2011; 40 (3): 305–316.
[79] Forero M, Yakovenko O, Sokurenko EV, Thomas WE, Vogel V, PLOS Biol, 2006; 4 (9): e298.
[80] Lugmaier RA, Schedin S, Kühner F, Benoit M, Eur. Biophys J, 2008; 37 (2): 111–120.
[81] Biais N, Higashi D, So M, Ladoux B, Methods Mol Biol Clifton NJ, 2012; 799: 197–216
[82] Maier B, Wong GCL, Trends Microbiol, 2015; 23 (12): 775–788
[83] Maier B, Soft Matter, 2013; 9 (24): 5667–5671.
[84] Merz AJ, So M, Sheetz MP, Nature, 2000; 407 (6800): 98–102.
[85] Allemand JF, Maier B, FEMS Microbiol Rev, 2009; 33 (3): 593–610.
[86] Marathe R, Meel C, Schmidt NC, Dewenter L, Kurre R, Greune L, Schmidt MA, Müller MJI, Lipowsky R, Maier B et al., Nat Commun, 2014; 5: 3759.
[87] Dufrêne YF,Trends Microbiol, 2015; 23 (6): 376–382
[88] Müller DJ, Helenius J, Alsteens D, Dufrêne YF, Nat. Chem. Biol., 2009, 5 (6), 383–390
[89] Formosa-Dague C, Feuillie C, Beaussart A, Derclaye S, Kucharíková S, Lasa I, Van Dijck P, Dufrêne YF, ACS Nano, 2016; 10 (3): 3443–3452.
[90] Herman-Bausier P, Formosa-Dague C, Feuillie C, Valotteau C, Dufrêne YF, J Struct Biol, 2017 ; 197(1) :65-69.
[91] Beaussart A, Baker AE, Kuchma SL, El-Kirat-Chatel S, O'Toole GA, Dufrêne YF, ACS Nano, 2014; 8 (10): 10723–10733
[92] Sullan RMA, Beaussart A, Tripathi P, Derclaye S, El-Kirat-Chatel S, Li JK, Schneider Y-J, Vanderleyden J, Lebeer S, Dufrêne YF, Nanoscale, 2014; 6 (2): 1134–1143
[93] Li G, Brun YV, Tang JX, BMC Microbiol, 2013 ; 13 : 139.
[94] Jacquot A, Sakamoto C, Razafitianamarahavo A, Caillet C, Merlin J, Fahs A, Ghigo JM, Duval JFL, Beloin C, Francius G, Nanoscale, 2014; 6:12665-12681.
[95] Potthoff E, Ossola D, Zambelli T, Vorholt JA, Nanoscale, 2015 ; 7 (9) : 4070–4079
[96] Ma L, Jackson KD, Landry RM, Parsek MR, Wozniak DJ, J Bacteriol, 2006; 188 (23): 8213–8221.
[97] Byrd MS, Pang B, Mishra M, Swords WE, Wozniak DJ, mBio, 2010; 1 (3): e00140-10.
[98] Gibiansky ML, Hu W, Dahmen KA, Shi W, Wong GCL, Proc Natl Acad Sci, 2013; 110 (6): 2330–2335

[99] Faure LM, Fiche J-B, Espinosa L, Ducret A, Anantharaman V, Luciano J, Lhospice S, Islam ST, Tréguier J, Sotes M et al., Nature, 2016; 539 (7630): 530–535
[100] Grumbein S, Werb M, Opitz M, Lieleg O, J Rheol, 2016; 60(6): 1085-1094.
[101] Körstgens V, Flemming H-C, Wingender J, Borchard W, J Microbiol Meth, 2001; 46(1): 9-17.
[102] He Y, Peterson BW, Jongsma MA, Ren Y, Sharma PK, Busscher HJ, van der Mei HC, Plos One, 2013 ; 8(5): e63750.
[103] Pavlovsky L, Sturtevant RA, Younger JG, Solomon MJ, Langmuir, 2015; 31: 2036.
[104] Ochoa J-O, Coufort C, Escudié R, Liné A, Paul E, Chem Eng Sci, 2007; 62: 3672.
[105] Shaw T, Winston M, Rupp CJ, Klapper I, Stoodley P, Phys Rev Lett, 2004; 93(9): 098102.
[106] Lieleg O, Caldara M, Baumgärtel R, Ribbeck K, Soft Matter, 2011;7: 3307-3314.
[107] Stoodley P, LewandowskiZ, Boyle JD, Lappin-Scott HM, Biotechnol Bioeng, 1999; 65(1): 83.
[108] Stoodley P, LewandowskiZ, Boyle JD, Lappin-Scott HM, Environ Microbiol, 1999; 1(5): 447.
[109] Aravas N, Laspidou CS, Biotechnol Bioeng, 2008; 101(1): 196.
[110] Vo GD, Heys J, Biotech Bioeng, 2011; 108(8): 1893.
[111] Blauert F, Horn H,Wagner M, Biotech Bioeng, 2015; 112(9): 1893.
[112] Wimpenny J,Manz W, Szewzyk U, FEMS Microbiol Rev, 2000; 24: 661-671.
[113] Hall-Stoodley L, Costerton JW, Stoodley P, Nature Reviews Microbiol, 2004; 2: 95-107.
[114] Battin TJ, Sloan WT, Kjelleberg S, Daims H, Head IM, Curtis TP, Eberl L, Nature, 2007; 5: 76-81.
[115] Drescher K, Shen Y, Bassler BL, Stone HA, Proc Natl Acad Sci USA, 2013; 110: 4345-4350.
[116] Rusconi R, Lecuyer S, Autrusson N, Guglielmini L, Stone HA, Biophys J, 2011; 100: 1392-1399.
[117] Thomas K, Herminghaus S, Porada H, Goehring L, Phil Trans R Soc A, 2013; 371: 20120362.
[118] Dogsa I, Brloznik M,Stopar D, Mandic-Mulec I, PLos ONE, 2013; 8(4): e62044.
[119] Hollenbeck EC, Fong JCN, Lim JY, Yildiz FH, Fuller GG, Cegelski L, Biophys J, 2014; 107: 2245-2252.
[120] Hollenbeck EC, Douarche C, Allain J-M, Roger P, Regeard C, Cegelski L, Fuller GG, Raspaud E, J Phys Chem B, 2016; 120: 6080.
[121] Stewart PS,Franklin MJ, Nature Rev Microbiol, 2008; 6: 199.
[122] Lopez D, Vlamakis H, Kolter R, Cold Spring Harb Perspect Biol, 2010; 2: a000398.
[123] Bridier A, Sanchez-Vizuete P, Guilbaud M, Piard JC, Naïtali M, Briandet R, Food Microbiol, 2015 ; 45(PtB) : 167-178.
[124] Douarche C, Allain J-M, Raspaud E, Biophys J, 2015; 109: 2195.
[125] Stewart PS, Murga R, Srinivasan R, de Beer D, Wat Res, 1995, 29(8),2006-2009.
[126] Cao H, Habimana O, Safari A, Heffernan R, Dai Y, Casey E, NPJ Biofilms Microbiomes, 2016; 2:5.
[127] Flemming HC, Wingender J, Szewzyk U, Steinberg P, Rice SA, Kjelleberg S, Nature Reviews Microbiol, 2016, 14, 563.
[128] Mah T-FC, O'Toole GA, Trends in Microbiol, 2001, 9(1), 34.
[129] Xu KD, Stewart PS, Xia F, Huang CT, Mc Feters GA, Appl Environ Microbiol, 1998, 64(10), 4035-4039.

[130] Galy O, Latour-Lambert P, Zrelli K, Ghigo JM, Beloin C, Henry N, Biophys J, 2012; 103: 1400-1408.
[131] Wang X, Han J, Li K, Wang G, Hao M, J Bioinform Comput Biol, 2016; 14(4), 1650014.
[132] Grant MAA, Waclaw B, Allen RJ, Cicuta P, J R Soc Interface, 2014; 11:20140400.
[133] Guégan C, Garderes J, Le Pennec G, Gaillard F, Fay F, Linossier I, Herry JM, Bellon Fontaine MN, Valée Réhel K, Colloids and Surfaces B: Biointerfaces, 2014; 114: 193.
[134] Duvernoy MC, Mora T, Ardré M, Croquette V, Bensimon D, Quilliet C, Ghigo JM, Balland M, Beloin C, Lecuyer S, Desprat N, to appear; http://biorxiv.org/content/early/2017/01/31/104679.
[135] Delarue M, Hartung J, Schreck C, Gniewek P, Hu L, Herminghaus S, Hallatscheck O, Nature Physics, 2016; 12: 762.
[136] Drescher K, DunkelJ, NadellCD, vanTeeffelen S, GrmjaI, Wingreen NS, Stone HA,Bassler BL, Proc Natl Acad Sci USA, 2016; E2066.
[137] Chew SC, Kundukad B, Teh WK, Doyle P, Yang L,Rice SA, Kjelleberg S, Soft Matter, 2016; 12: 5224.
[138] Trejo M, Douarche C, Bailleux V, Poulard C, Mariot S, Regeard C, Raspaud E, Proc Natl Acad Sci USA, 2013; 110(6): 2011.
[139] Asally M, Kittisopikul M, Rué P, Du Y, Hu Z, Çağatay T, Robinson AB, Lu H, Garcia-Ojalvo J, Süel GM, Proc Natl Acad Sci USA, 2012; 109(46): 18891.
[140] Wilking JN, Zaburdaev V, De Volder M, Losick R, Brenner MP, Weitz DA, Proc Natl Acad Sci USA, 2013; 110(3): 848.
[141] Serra DO, Klauck G, Hengge R, Environ Microbiol, 2015; 17(12): 5073.
[142] Ben Amar M, Wu M, Europhys Lett, 2014; 108: 38003.
[143] Espeso DR, Carpio A, Einarsson B, Phys Rev E, 2015; 91: 022710.
[144] Zhang C, Li B, Huang X, Ni Y, Feng XQ, Appl Phys Lett, 2016; 109: 143701.
[145] Flemming HC, Wingender J, Nat Rev Microbiol, 2010; 8:623-633.
[146] Berk V, Fong JC, Dempsey GT, Develioglu ON, Zhuang X, Liphardt J, Yildiz FH, Chu S, Science, 2012 ; 337(6091):236-239.
[147] De Gennes PG. Scaling Concepts in Polymer Physics, Ithaca, Cornell University Press; 1979.
[148] Doi M and SF Edwards. The Theory of Polymer Dynamics, New York, Oxford University Press; 1986.
[149] Panyukov S, Rabin Y, Phys Rep, 1996; 269(1-2): 1-131.
[150] Mendes E, Lindner P, Buzier M, Boue F, Bastide J, Phys Rev Lett, 1991; 66(12): 1595-1598.
[151] Shibayama M, Macromol Chem Physic, 1998; 199(1): 1-30.
[152] Munch JP, Candau S, Herz J, Hild G, J Phys-Paris, 1977; 38(8): 971-976.
[153] Llorente MA, Andrady AL, Mark JE, J Polym Sci Pol Phys, 1981; 19(4): 621-630.
[154] Mark JE, Adv Polym Sci, 1982; 44: 1-26.
[155] Bastide J, Leibler L, Macromol, 1988; 21(8): 2647-2649.
[156] Flory PJ, Rehner J, J Chem Phys, 1943; 11(11): 512-520.
[157] Flory PJ, Rehner J, J Chem Phys, 1943; 11(11): 521-526.
[158] James HM, Guth E, J Chem Phys, 1943; 11(10): 455-481.
[159] Obukhov SP, Rubinstein M, Colby RH, Macromol, 1994; 27(12): 3191-3198.
[160] Mi L, Licina GA, Jiang S, ACS Sustainable Chem Eng, 2014; 2: 2448-2453.
[161] Csonka LN, Microbiol Rev, 1989; 53:121-147.
[162] Prigent-Combaret C, Vidal O, Dorel C, Lejeune P, J Bacteriol, 1999; 181: 5993-6002.

[163] Seminara A, Angelini TE, Wilking JN, Vlamakis H, Ebrahim S, Kolter R, Weitz DA, Brenner MP, Proc Natl Acad Sci USA, 2012; 109: 1116-1121.
[164] Bertrand T, Peixinho J, Mukhopadhyay S, MacMinn CW, Phys Rev Appl, 2016 ; 6 : 064010.
[165] Li K, Ding K, Cai S, Appl Phys Lett, 2013; 102: 241908.
[166] Mora T, Boudaoud A, Eur Phys J E, 2006; 20:119-124.
[167] Dervaux J, Ben Amar M, Annu Rev Condens Matter Phys, 2011; 3:311-332.
[168] Li B, Cao YP, Feng XQ, Gao H, Soft Matter, 2012; 8:5728-5745.
[169] Peak CW, Wilker JJ, Schmidt G, Colloid Polym Sci, 2013; 291(9): 2031-2047.
[170] Zhao X, Soft Matter 2014; 10(5): 672-687.
[171] Okumura Y, Ito K, Adv Mater, 2001; 13(7): 485.
[172] Sakai T, Matsunaga T, Yamamoto Y, Ito C, Yoshida R, Suzuki S, Sasaki N, Shibayama M and Chung UI, Macromol, 2008; 41(14): 5379-5384.
[173] Akagi Y, Sakurai H, Gong JP, Chung UI, Sakai T, J Chem Phys, 2013 ; 139(14): 144905.
[174] Gong JP, Katsuyama Y, Kurokawa T, Osada Y, Adv Mater, 2003; 15(14): 1155-1158.
[175] Nakajima T, Furukawa H, Tanaka Y, Kurokawa T, Osada Y, Gong JP, Macromol, 2009; 42(6): 2184-2189.
[176] Gong JP, Soft Matter, 2010; 6(12): 2583-2590.
[177] Zheng WJ, Liu ZQ, Xu F, Gao J, Chen YM, Gong JP, Osada Y, Macromol Chem Physic, 2015; 216(6): 641-649.
[178] Ducrot E, Chen Y, Bulters M, Sijbesma RP, Creton C, Science, 2014; 344(6180): 186-189.
[179] Sun JY, Zhao XH, Illeperuma WRK, Chaudhuri O, Oh KH, Mooney DJ, Vlassak JJ, Suo ZG, Nature, 2012; 489(7414): 133-136.
[180] Haraguchi K, Takehisa T, Fan S, Macromol, 2002; 35(27): 10162-10171.
[181] Haraguchi K, Li HJ, Macromol, 2006; 39(5): 1898-1905.
[182] Haraguchi K, Li HJ, J Polym Sci Pol Phys, 2009; 47(23): 2328-2340.
[183] Gaharwar AK, Rivera CP, Wu CJ, Schmidt G, Acta Biomater, 2011; 7(12): 4139-4148.
[184] Wang T, Liu D, Lian CX, Zheng SD, Liu XX, Tong Z, Soft Matter, 2012; 8(3): 774-783.
[185] Shibayama M, Soft Matter, 2012; 8: 8030-8038.
[186] Carlsson L, Rose S, Hourdet D, Marcellan A, Soft Matter, 2010; 6(15): 3619-3631.
[187] Rose S, Dizeux A, Narita T, Hourdet D, Marcellan A, Macromol, 2013 ; 46(10): 4095-4104.
[188] Nishida T, Endo H, Osaka N, Li H, Haraguchi K, Shibayama M, Phys Rev E, 2009; 80(3): 030801.
[189] Rose S, Prevoteau A, Elziere P, Hourdet D, Marcellan A, Leibler L, Nature, 2014 ; 505: 382-385.
[190] Meddahi-Pelle A, Legrand A, Marcellan A, Louedec L, Letourneur D, Leibler L, Angewandte Chemie- Int. Ed., 2014 ; 53: 1-6.
[191] Koo H, Yamada KM, Curr Opin Cell Biol, 2016; 42:102–12.
[192] Chen H, Zhao X, Lu X, Kassab G, Int J Nonlin Mech 2013; 56: 79–85.
[193] Sherman VR, Yang W, Meyers MA, J Mech Behav Biomed 2015; 52: 22–50.
[194] Fung YC. Biomechanics. Mechanical Properties of Living Tissues. second edition. Springer-Verlag; 1993.
[195] Lanir Y, J Biomech, 1983; 16: 1–12.
[196] Frantz C, Stewart KM, Weaver VM, J Cell Sci, 2010; 123: 4195–200.
[197] Abrahams M, Med Biol Eng, 1967; 5: 433–443.

[198] Veronda DR, Westmann RA, J Biomech, 1970; 3: 111–124.
[199] Holzapfel GA, Gasser TC, Ogden RW, J Elasticity, 2000; 61: 1–48.
[200] Lanir Y, Lokshin O, J Biomech Eng, 2009; 131: 031009.
[201] Kang G, Wu X, J Mech Behav Biomed, 2011; 4: 498–506.
[202] Goulam Houssen Y, Gusachenko I, Schanne-Klein M-C, Allain J-M, J Biomech, 2011; 44: 2047–52.
[203] Caro-Bretelle AS, Gountsop PN, Ienny P, Leger R, Corn S, Bazin I, et al. J Biomech, 2015; 48: 3135–41.
[204] Brown IA, Brit J Dermatol, 1973; 89: 383–93.
[205] Puxkandl R, Zizak I, Paris O, Keckes J, Tesch W, Bernstorff S, et al, Philos T Roy Soc B, 2002; 357: 191–7.
[206] Hansen KA, Weiss JA, Barton JK, J Biomech Eng, 2002; 124: 72.
[207] Gupta HS, Seto J, Krauss S, Boesecke P, Screen HRC, J Struct Biol, 2010; 169: 183–91.
[208] Bancelin S, Lynch B, Bonod-Bidaud C, Ducourthial G, Psilodimitrakopoulos S, Dokládal P, et al, Sci Rep, 2015; 5: 17635.
[209] Benoit A, Latour G, Marie-Claire S-K, Allain J-M, J Mech Behav Biomed, 2015; 60: 93-105.
[210] Humphrey JD, Proc Math Phys Eng Sci, 2003; 459: 3–46.
[211] Avril S, Evans S, editors. Material Parameter Identification and Inverse Problems in Soft Tissue Biomechanics. vol. 573. Cham: Springer International Publishing; 2017.
[212] Bischoff JE, Ann Biomed Eng, 2006; 34: 1164–72.
[213] Sverdlik A, Lanir Y, J Biomech Eng 2002; 124: 78.
[214] Jones GW, Chapman SJ, SIAM Review, 2012; 54: 52–118.
[215] Delarue M, Montel F,Vignjevic D, Prost J, Joanny JF, Cappello G, Biophys J, 2014; 107: 1821–1828.
[216] Skalak R, Zargaryan S, Jain RK, Netti PA, Hoger A, J Math Biol, 1996; 34: 889–914.
[217] Rodriguez EK, Hoger A, McCulloch AD, J Biomech, 1994; 27: 455–67.
[218] Taber LA, Eggers DW, J Theor Biol, 1996; 180: 343–357.
[219] Zöllner AM, Holland MA, Honda KS, Gosain AK, Kuhl E, J Mech Behav Biomed, 2013; 28: 495–509.
[220] Goriely A, Weickenmeier J, Kuhl E, Phys Rev Lett, 2016; 117: 138001.
[221] Ambrosi D, Mollica F, J Math Biol, 2004; 48: 477–99.
[222] Ben Amar M, Jia F, Proc Natl Acad Sci USA, 2013; 110: 10525–30.
[223] Vandiver R, Goriely A, Europhys Lett EPL, 2008; 84: 58004.
[224]Ben Amar M, Goriely A, J Mech Phys Solids, 2005; 53: 2284–319.
[225] Zöllner AM, Buganza Tepole A, Kuhl E, J Theor Biol, 2012; 297: 166–75.
[226] Humphrey JD, Dufresne ER, Schwartz MA, Nat Rev Mol Cell Biol, 2014; 15: 802–12.
[227] Goriely A, Amar MB, Biomech Model Mechanobiol, 2007; 6: 289–96.
[228] Humphrey JD, Rajagopal KR, M M M A S, 2002; 12: 407–30.
[229] Moulia B, Coutand C, Lenne C, Am J Bot, 2006; 93: 1477–1489.
[230] Ben Amar M, Allain J-M, Puff N, Angelova M, Phys Rev Lett, 2007; 99(4): 040401.
[231] Delarue M, Joanny JF, Julicher F, Prost J, Interface Focus, 2014; 4: 20140033–20140033.
[232] Drasdo D, Adv Complex Syst, 2005; 08: 319–63.
[233] Whitney JC, Howell PL, Trends in Microbiol, 2013; 21(2):63-72.
[234] Dajkovic A et al, Molecular Microbiology, 2017; 104(6): 972–988.
[235] Thwaites J. J, Mendelson N. H, Proc Natl Acad Sci USA, 1985; 82: 2163-2167.

[236] Mendelson N. H, Sarlls J. E, Wolgemuth C.W, Goldstein R. E, Phys Rev Lett, 2000; 84: 1627-1630.
[237] Pelling A. E, Li Y, Shi W, Gimzewski J. K, Proc Natl Acad Sci USA, 2005; 102: 6484-6489.
[238] Holland D. P, Walsby A. E, Journal of Microbiological Methods, 2009; 77: 214-224.
[239] Arnoldi M, Fritz M, Bäuerlein E, Radmacher M, Sackmann E, Boulbitch A, Phys Rev E, 2000; 62: 1034-1044.
[240] Yao X, Walterc J, S. Burke S, S. Stewart S, Jericho M. H, D. Pink D, R. Hunter R, Beveridge T. J, Colloids and Surfaces B: Biointerfaces, 2002; 23: 213-230.
[241] Swift Jet al., Science, 2013; 341:1240104.

Table 1: Typical values of some mechanical parameters measured by different methods on single bacteria.

Parameter	Method	Bacteria	Typical Values /Range	References
Young Modulus	mostly AFM, optical tweezers, microfluidic devices	Different species and strains	Few kPa to several MPa	[16,25,44,45,56, 234,235,236,237]
Young Modulus variation along a single bacterium	AFM	*Anabaenopsis circularis* *Rhodococcus wratislaviensis*	10-60 kPa	[18]
Turgor Pressure	AFM indentation Collapse gas vesicles Simulation	*E. coli* *Streptococci* *Pseudomonas aeruginosa* *Enterococcus hirae* *Magnetospirillum gryphiswaldense*	10-400 kPa	[31,50,51,238-240]
Lytic Membrane Tension	Patch-clamp	*E. coli*	15 mN/m	[53,55]
Pili stiffness	AFM	*E. coli*	0.1 pN/m	[72,73]

Table 2: Typical values of Young's moduli measured on different systems.

Systems	Typical Young Modulus (kPa) or observed variation of Young moduli	References
Biofilms grown on liquid susbstrate	0.3	[138]
Biofilms grown on solid substrates	Few kPa to several MPa	[16]
variation of Young moduli along one single biofilm	by a factor of 10	[126,130]
Hydrogels	$1 - 10^3$	[183]
Brain, bone marrow	0.2 - 1	[241]
Cartilage	30	[241]
Skin (mice)	10^3	[208]
Tendon	$10^5 - 2\ 10^6$	[213]

Figure Captions

Figure 1: A) Macroscopic *Escherichia coli* biofilm formed on Pyrex glass slide after 24H culture in a biofilm micro fermenter. The white material corresponds to millimeter-thick biofilm biomass; B) 3D structure of a mixed biofilm formed by fluorescent *Bacillus subtilis* (green) and *Staphylococcus aureus* (red) observed by confocal laser scanning microscopy [6] - scale bar 50 μm. The extracellular matrix is not stained and therefore not visible here; C) Biofilm of a mutated *E. coli* observed by scanning electron microscopy after fixation, staining and dehydration [7]. The black C arrow indicates overlap of different secreted protein fibers. Copyright permission in progress.

Figure 2: A) Typical Force-Indentation curves obtained by AFM on isolated living bacteria without (blue) and with antibiotics (green and red) [19]. B-C) Example of stiffness mapping

extracted from AFM analysis on three living bacteria *Rhodococcus wratislaviensis* standing on a rigid substrate. B) Colors represent different heights from the substrate. C) Zoom of the square region in B) showing the stiffness map [18]. Copyright permission in progress.

Figure 3: A) Model of stored growth in *E. coli*. Bars and spheres represent glycan strands, peptide cross-links and peptidoglycan synthetic machinery, followed by buckling and/or extension depending on the turgor pressure [35]. B) Force indentation curves obtained by probing a *E. coli* cell and a bulge. Inset (c): a bulging cell labeled by cytoplasmic GFP probes and observed by fluorescence microscopy [46]. C) Daughter cell separation in *S. aureus* as imaged by Scanning Electron Microscopy; scale bar 1 micrometer [47]. D) Stress distribution in the "ready-to-pop" cell wall modeled as a finite elastic material and expressed in relative unit [47]. Copyright permission in progress.

Figure 4: Typical rheological experiments performed on macroscopic biofilms. A) Response of a *Staphylococcus aureus* biofilm to a shear stress (loading and unloading) [12]. B) Response of a *Staphylococcus epidermis* to an oscillating strain (deformation); Elastic or storage (G', blue data) and viscous or loss (G'', red data) moduli are plotted as a function of the oscillation frequency [103]. Copyright permission in progress.

Figure 5: A) Macro-colony biofilm of *Salmonella sp.* grown on congo red and blue comassie agar gel revealing the genetic diversification. Image size 1.7 x 1.7 cm [123]; B) lateral xy-mapping of the creep compliance (in Pa^{-1} unit) of *Pseudomonas fluorescens* biofilm as extracted from fluorescent bead-tracking [126]; C) Occurrence of the different behaviors

measured when embedding probes at different locations inside a F pilus expressing *E. coli* biofilm. D) Values of the local mean compliance J_0 (averaged over 3 measurements performed within 7 μm – slices) and of its standard deviation as a function of the distance from the substrate. Figures C & D) are reprinted from [130].

Figure 6: A) Stress-strain curve performed on a flat pellicle of *Bacillus subtilis* (NCIB3610). The force was measured during uniaxial elongation and the strain was determined from an analysis of the deformation field [120]. B) Part of a pellicle starting to form wrinkles (top view): at the bottom side, the pellicle is confined and subjected to compressive stress along its two axes of confinement while at the top side the pellicle is only subjected to the compressive stress in one direction after suppressing the confinement effect in the other direction. Copyright permission in progress.

Figure 7: A) wrinkled and folded biofilms of E.coli (AR3110 strain) grown on an agar gel after two days of incubation [141]. B) Bacillus subtilis biofilm grown on agar gel after three-days of incubation; wrinkles and buckling, facilitated by the presence of dead cells, in the central area of the biofilm [139] and C) SEM (Scanning Electron Microscopy) image of a radial fold cross-section [140]. D) In silico biofilm showing radial wrinkles emerging from the central cores [143]. Copyright permission in progress.

Figure 8: Sequence of images showing a swelling hydrogel sphere [165]. The outer layer in direct contact with water expands more than does the inner core generating mechanical

constrains and buckling few times after the immersion. The instability patterns disappear when the spherical gel reaches the equilibrium state. Copyright permission in progress.

Figure 9: Schematic representation of local network structures of tough hydrogel: slide-ring gels (a,[171]), tetra-PEG gels (b, [172]), double-network gels (c) and nanocomposite gels (d,[185]). Adapted from Ref. [169]. Copyright permission in progress.

Figure 10: Use of rigid silica Nanoparticules (NP) in hydrogels: reinforcement A) & B), and gluing C). A) Hybrid networks combine exchangeable bonds (symbolized by arrows, here by polymer adsorption, silica NPs act as exchangeable cross-links) and permanent chemical cross-links (dots). Typical gel may contain 90 % of water and are filled with various volume fractions *x* v/v of silica NPs. B) Effect of NPs on the large strain mechanical behaviour. As a guideline, the pure chemical gel response (without NP). C) Gluing gels by NP solutions: schematic illustration of the concept of gluing two gels of the same or different natures together using nanoparticles. Network chains are adsorbed on nanoparticles and anchor particles to gel pieces. Particles act as connectors between gel surfaces and adsorbed chains also form bridges between particles. In adsorbed gel layers, at equilibrium or under tension, there is a constant traffic of monomers between the adsorbed and desorbed states, and rearrangements may adsorb and replace the detached link. Such exchange processes and rearrangements allow for large deformations and energy dissipation under stress. Copyright A) and B) Ref. [187]. C) from [189]. Copyright permission in progress.

Figure 11: Collagen organization in skin (A) and in tendon (B). A) SEM image of the human dermis, showing the collagen fibers (bar = 5µm) [233]. B) Multiphoton Mmicroscopy image of rat tail tendon, showing only the collagen fibers (bar = 50µm) [202]. Copyright permission in progress.

Figure 12: Force vs strain curve for human skin. The curve is classically split into 3 regions: the phase 1 or "toe", the phase 2 or "heel" and the phase 3 or linear. Vignettes are SEM images, showing the collagen fibers. Image from [204]. Copyright permission in progress.

Figure 13: Logged tree which has cracked due to the release of residual (or growth) stress. Picture taken from [214]. Copyright permission in progress.

Figure 14: Decomposition of the geometric deformation tensor F into a first growth tensor G and an elastic deformation tensor A. Figure from [224]. Copyright permission in progress.

Figure 1

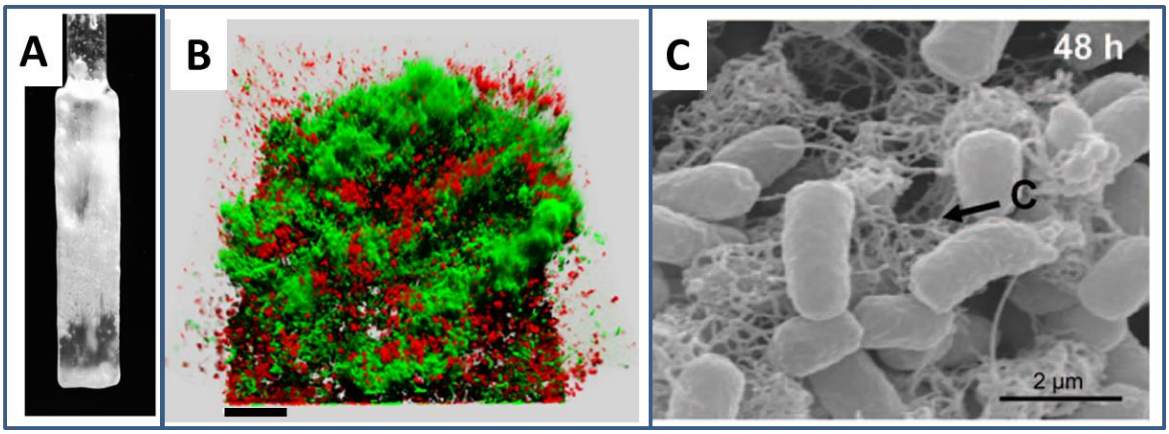

Figure 2

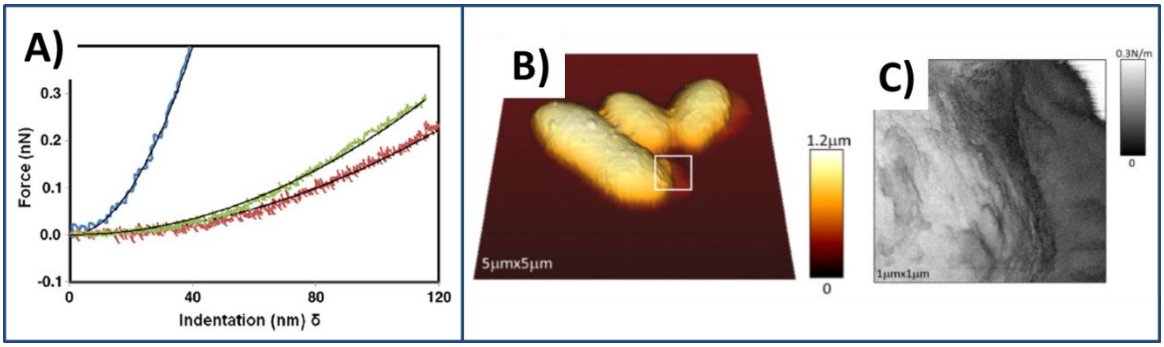

Figure 3

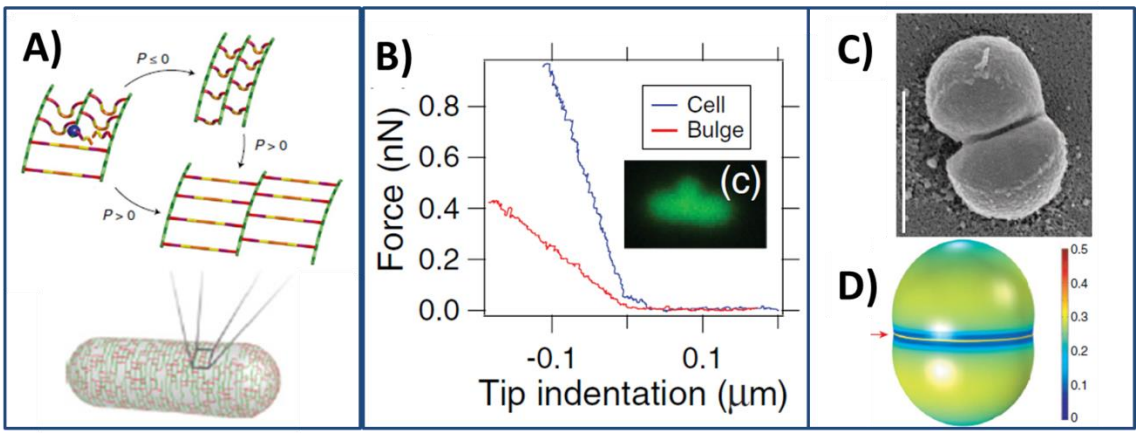

Figure 4

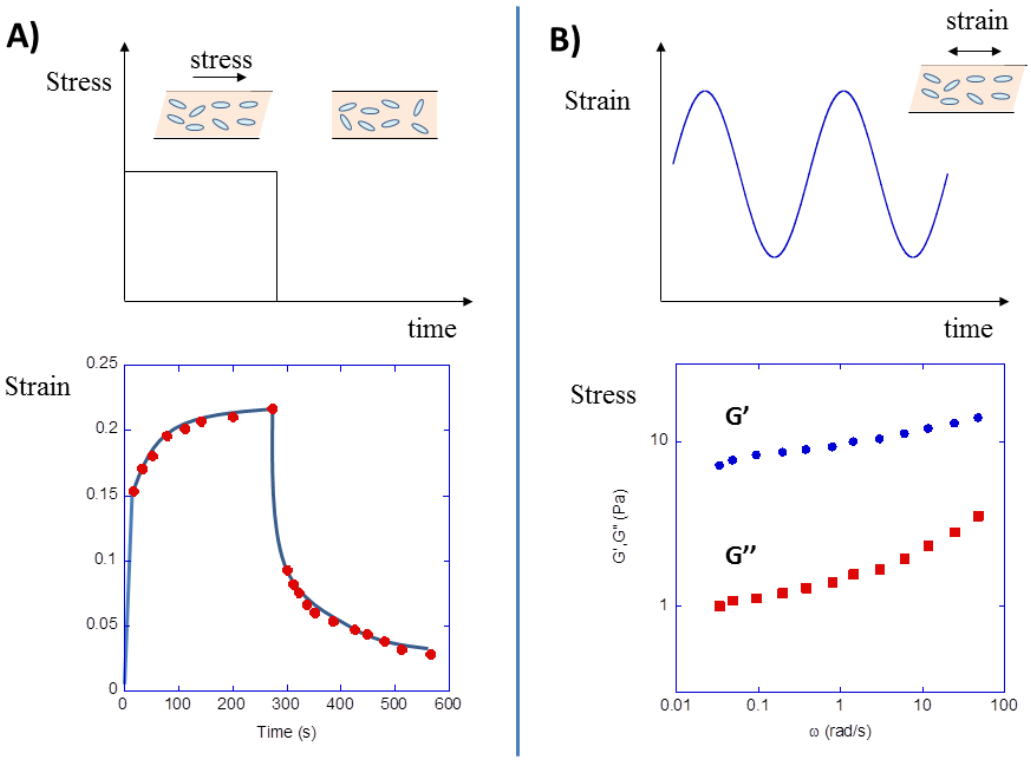

Figure 5

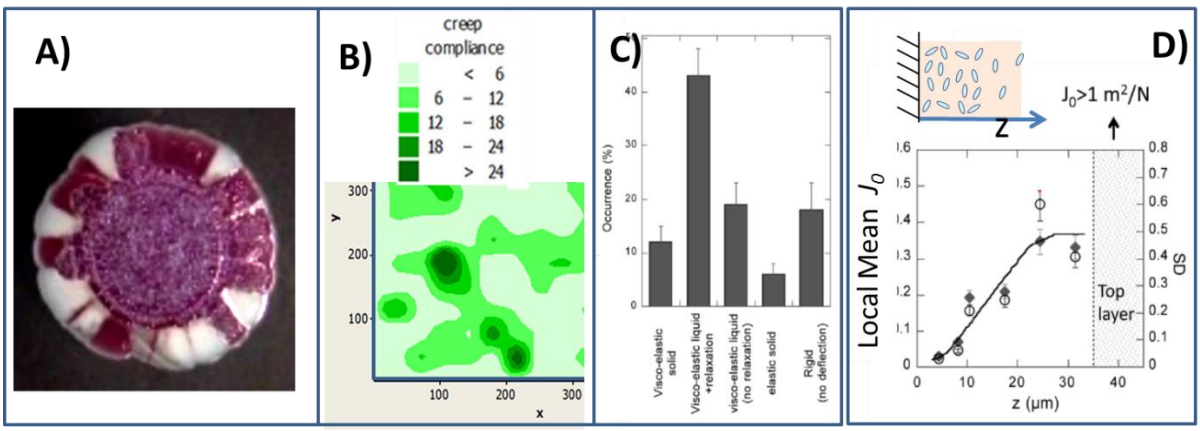

Figure 6

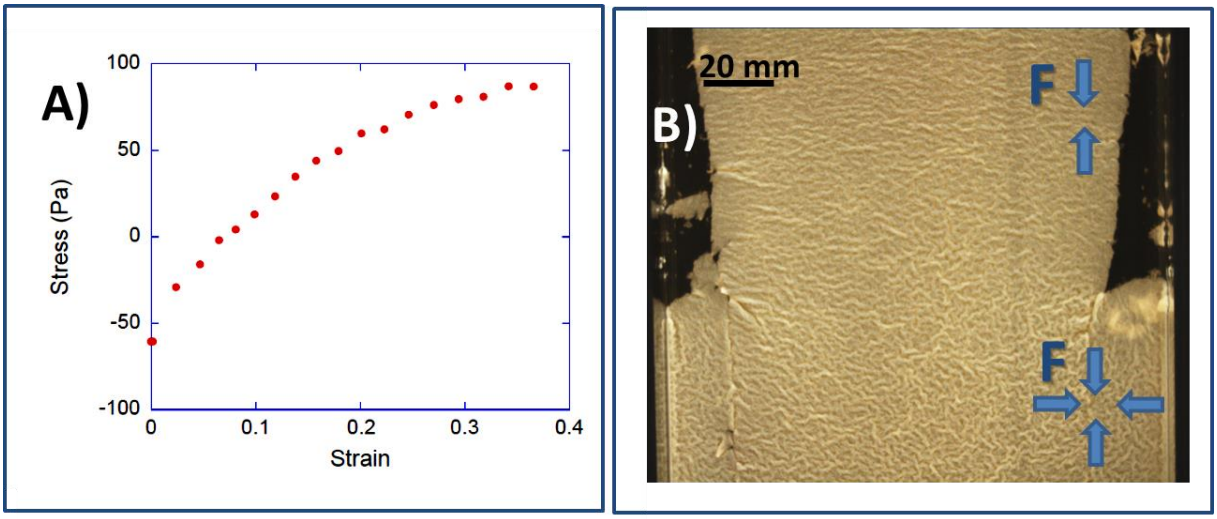

Figure 7

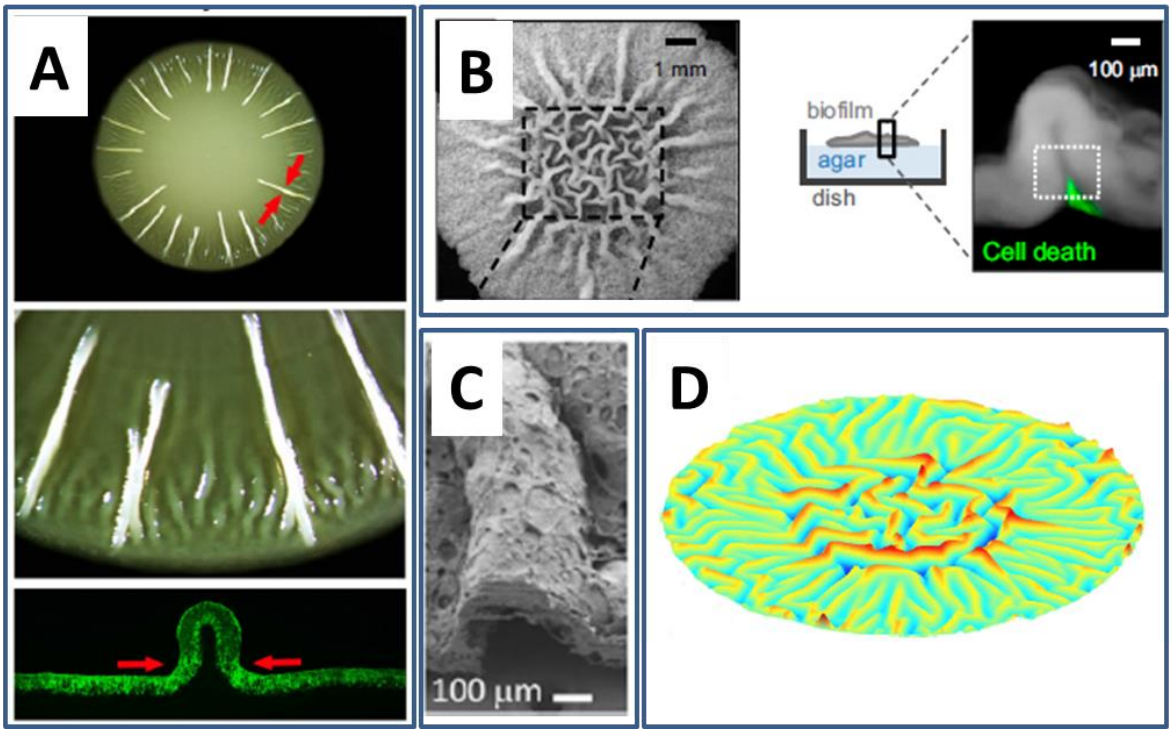

Figure 8

Figure 9

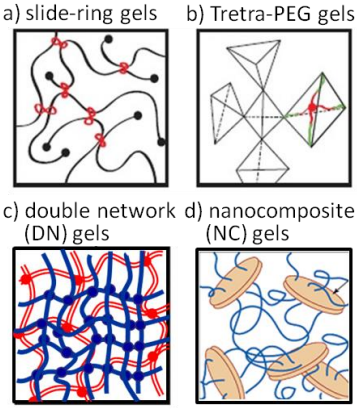

Figure 10

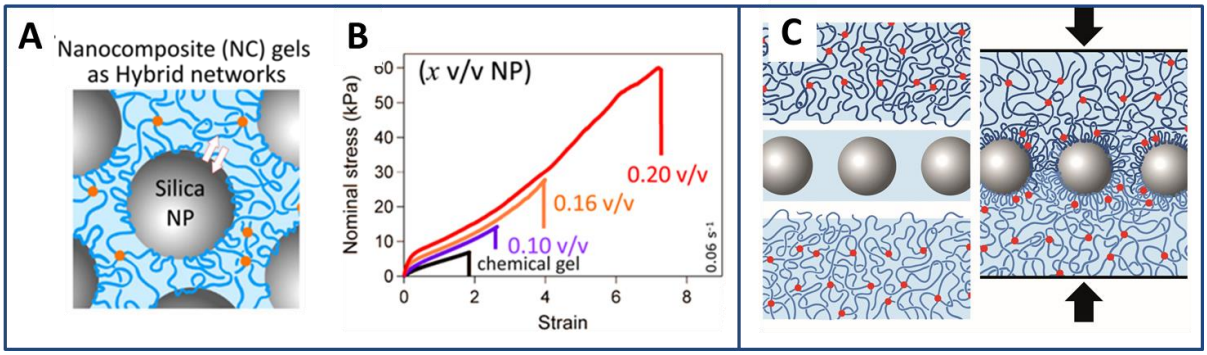

Figure 11

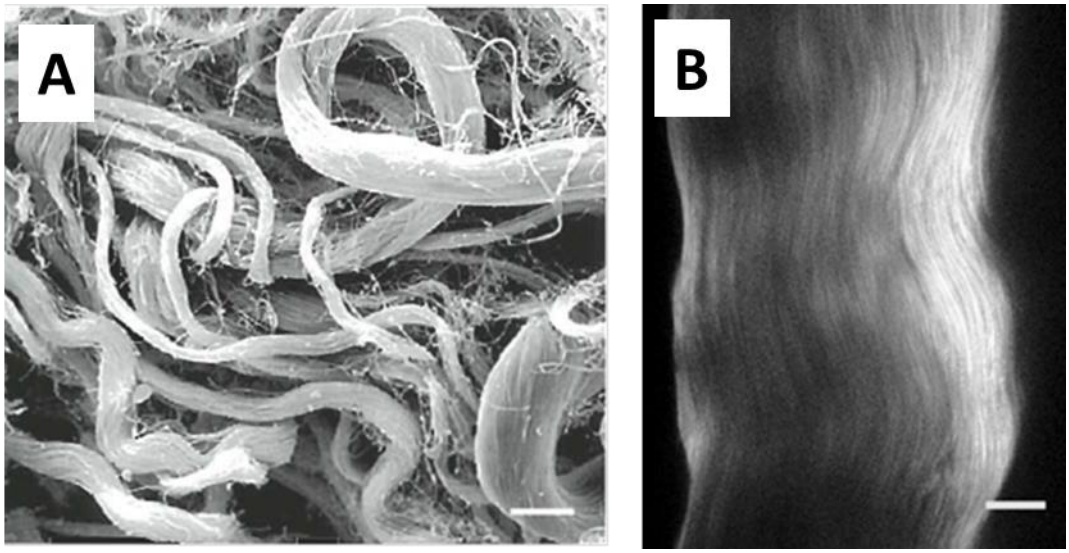

Figure 12

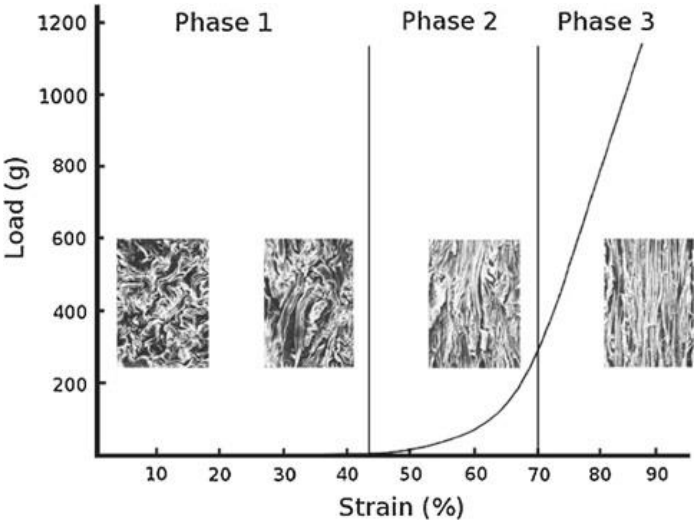

Figure 13

Figure 14